Wind waves in the North Atlantic from ship navigational radar: SeaVision development and its validation with Spotter wave buoy and WaveWatch III

Natalia Tilinina[1,2], Dmitry Ivonin[1], Alexander Gavrikov[1], Vitali Sharmar[1], Sergey Gulev[1,3], Alexander Suslov[1], Vladimir Fadeev[4], Boris Trofimov[4], Sergey Bargman[4], Leysan Salavatova[5], Vasilisa Koshkina[5], Polina Shishkova[1], Elizaveta Ezhova[5], Mikhail Krinitsky[1], Olga Razorenova[1], Klaus Peter Koltermann[6], Vladimir Tereschenkov[1] and Alexey Sokov[1]

[1] Shirshov Institute of Oceanology, RAS, Nakhimovsky ave. 36, 117997, Moscow, Russia

[2] Université Grenoble Alpes, CNRS, IRD, Grenoble-INP, Institut des Géosciences de l'Environnement, 70 rue de la Physique, 38400, Grenoble, France

[3] A.M. Obukhov Institute of Atmospheric Physics, RAS, Pyzhevskiy Lane 3, Moscow, 109017, Russia

[4] Joint stock company "Marine Complexes and Systems", Aleksandrovskoy Fermy ave. 2 office 2H, 192174, Saint-Petersburg, Russia

[5] Moscow Institute of Physics and Technology, Institutskiy Pereulok 9, 141701, Dolgoprudny, Moscow Region, Russia

[6] Lomonosov Moscow State University, Moscow Russia

Correspondence to: Natalia Tilinina (tilinina@sail.msk.ru) and Alexander Gavrikov (gavr@sail.msk.ru)

Abstract

Wind waves play an important role in the climate system, modulating the energy exchange between the ocean and the atmosphere and effecting ocean mixing. However existing ship-based observational networks of wind waves are still sparse limiting therefore the possibilities of validating satellite missions and model simulations. In this paper we present data collected on three research cruises in the North Atlantic and Arctic in 2020 and 2021 and the SeaVision system for measuring wind wave characteristics over the open ocean with a standard marine navigation X-band radar. Simultaneously with SeaVision wind wave characteristics measurements we also collected data from the Spotter wave buoy in the same locations and ran the WaveWatch III model in a very high-resolution configuration over the observational domain. After the quality control, SeaVision measurements were validated against co-located Spotter wave buoy data and intercompared with the output of WaveWatch III simulations. Observations of the wind waves with the navigation X-band radar were found to be in agreement with buoy data and model simulations with the best match for the wave propagation directions. Supporting datasets consist of significant wave heights, wave periods and wave energy frequency spectra derived from both SeaVision

Natalia 26.6.2022 12:53

Удалено: The global coverage of the observational network of the wind waves is still characterized by the significant gaps in *in situ* observations. At the same time wind waves play an important role into the Earth' climate system specifically in the air-sea interaction processes and energy exchange between the ocean and the atmosphere. In this paper we present the SeaVision system for measuring wind waves' parameters in the open ocean with navigational marine X-band radar and prime data collection from the three research cruises in the North Atlantic (2020 and 2021) and Arctic (2021). Simultaneously with SeaVision observations of the wind waves we were collectingcollected data in the same locations and time with Spotter wave buoy and running WaveWatch III model over our domains. Measurements with SeaVision were quality controlled and validated by comparison with Spotter wave buoy data, in addition we run and WaveWatch III experiments for the domains of research cruises.. Observations of the wind waves with navigational X-band radar are in agreement among these three sources of data, with the best agreement for wave propagation directions. The dataset that supports this paper consists of significant wave height, wave period and wave energy frequency spectrum from both SeaVision and Spotter buoy avaiable through the PANGAEA repository (Gavrikov et al., 2022) at https://doi.pangaea.de/10.1594/PANGAEA.939620. The dataset can be used for validation of satellite missions as well as model outputs. One of the major highlights in this study is potential of all ships navigating into the open ocean and equipped with X-band marine radar to participate into the development of another observational network for the wind waves in the open ocean once cheap and independently operating version of the SeaVision (or any other system) is available.

and the Spotter buoy. All supporting data are available through the PANGAEA repository (Gavrikov et al., 2022) at https://doi.pangaea.de/10.1594/PANGAEA.939620. The dataset can be further used for validation of satellite missions and regional wave model experiments. Our study shows the potential of ship navigation X-band radars (when assembled with SeaVision or similar systems) for the development of a new near-global observational network providing a much larger amount of wind wave observations compared to e.g. Voluntary Observing Ship (VOS) data and research vessel campaigns.

1 Introduction

Ocean wind waves play a critically important role in air-sea energy and gas exchanges (Gulev and Hasse 1998; Andreas et al. 2015; Blomquist et al. 2017; Ribas-Ribas et al. 2018; Cronin et al. 2019; Xu et al. 2021 among many others) and in ocean surface mixing (McWilliams and Fox-Kemper 2013; Buckingham et al. 2019; Studholme et al. 2021), thus being an important active component of the coupled climate system (Cavaleri et al. 2012; Fan and Griffies 2014). At the same time massive long-term observations of wind waves over global oceans still have an insufficient coverage and quality compared to other surface variables (e.g. air and sea surface temperatures). Visual wave observations from Voluntary Observing Ships (VOS) while providing the longest time coverage (formally going back to the mid 19th century) suffer from space- and time dependent sampling biases as well as from both random and systematic biases and require continuous validation (Gulev et al. 2003). Remote sensing datasets of wind waves go back to 1985 (Ribal and Young, 2019), when the first satellite radar altimeters were launched and started to provide ocean surface elevations with high temporal and spatial resolution. However remote sensing data have to be validated against *in situ* measurements, typically available from buoys (such as NDBC buoys, Swail et al. 2010 or NOWPHAS, Nagai et al. 2005). Buoys measure vertical and horizontal displacements of the ocean surface (such as Spotter or Datawell buoys with up to 2.5 Hz sampling frequency, Raghukumar et al., 2019) and provide highly accurate estimates of wind waves characteristics, effectively assimilated into Numerical Weather Prediction (NWP) models. However, buoy networks are sparse with most deployments being in the coastal regions and can only effectively serve for verification of all other dataset rather than for developing global or regional climatologies.

Natalia 26.6.2022 13:09

Удалено: The history of wind waves studies in the ocean demonstrated a critically important role of the wind waves into the climate system, specifically in air-sea interaction processes and energy exchange between the ocean and the atmosphere. At the same time, the history of building a robust global and regional datasets for assessment of the wind waves climatology and dynamics revealed that the wave fields are always hard to measure both remotely and in situ with sufficient temporal and spatial resolutions to cover global and regional domains (comparing with e.g. air temperature or sea surface temperature). ... [1]

Starting from the 1980s considerable progress in wind wave modelling (WAMDI, 1988; Hasselmann et al., 1985; Cavaleri et al., 2020) resulted over the last decade in the development of multiple global and regional wind wave hindcasts generated by spectral wave models such as WAM (WAMDI 1988) or WAVEWATCH (WW3DG 2019) forced by atmospheric reanalyses or climate models and providing multidecadal wind wave fields with high temporal and spatial resolution (Casas-Prat et al., 2018; Semedo et al., 2018; Morim et al. 2020, 2022; Sharmar et al. 2021 among others). Being currently a widely accepted source for estimating long-term climate variability in wave characteristics, wind wave hindcasts also suffer from the inaccuracy of modelling of many aspects of wind wave dynamics, including e.g. extremely high wave peaks at high wind speeds during the storm passage (Cavaleri et al., 2020).

Summarizing, all three sources of global wind wave information (VOS, satellite data and model hindcasts) require data for extensive validation. Existing wave buoys deployed in a few locations can not solve this problem to a full extent. Thus,

Natalia 26.6.2022 13:15

Удалено: An important operational task is delivery of the wave forecast to the ships in the open ocean, which is typically (i) not very operational and (ii) not very accurate during the rough sea conditions. Thus, within this paper we present results of development and validation of the SeaVision system for (i) wind waves observations in the open ocean using navigational marine X-band radar and (ii) to monitor in real time wave heights, direction and period along the ship track in the open ocean.

investigating alternative sources of massive wind wave data remains a challenge. In this respect ship navigation radars represent an option whose potential, especially in open ocean regions, is not yet explored to a full extent. Here we present the results of the development and validation of the SeaVision system for wind wave observations in the open ocean using standard navigation marine X-band radars which allows for real time monitoring of wind wave characteristics along the commercial ship tracks.

Applicability of the navigation radars for measurements of the wind wave characteristics was first noted by Young et al. (1985). Radar images of the ocean surface, known as sea clutter, are generated by the Bragg scattering (Crombie, 1955) of the electromagnetic signal by the ripples on the ocean surface produced by the wind. Being emitted from the radar, an electromagnetic signal reaches the ocean surface and further, being reflected by ripples on the ocean surface, is received back by the radar antenna when the ocean surface is rough enough (i.e. ripples are developed). Under a wind speed > 3 m/s and waves height > 0.5 m the surface waves field becomes detectable on the radar image of the sea clutter (Hatten et al., 1998; Hessner and Hanson, 2010). Time sequences of these images are further analyzed for estimating of wind wave characteristics. The associated retrieval procedures can be based on various approaches, which include signal-to-noise ratio derived from the image spectrum (Nieto-Borge et al., 1999; Neito-Borge et al., 2008; Seemann et al., 1997), statistical analysis of the island-to-trough ratio on the sea clutter images (Buckley and Alter, 1997; Buckley and Alter, 1998), analysis of the image texture (Gangeskar, 2000), wavelet technique (Huang and Gill, 2015), the least square approach (Huang et al., 2014) and shadowing analysis (Gangeskar, 2014; Liu et al., 2015). Methodologies may also be based on the combination of these methods with the use of artificial neural networks (Vicen-Bueno et al., 2012 This may also include the analysis of the Doppler shift of the received radar signal that is based on the well-defined relationship between orbital velocities and wave height for linear gravity waves (Plant, 1997; Plant et al., 1987; Johnson et al., 2009; Hwang et al., 2010; Hackett et al., 2011; Chen et al., 2019). There are many aspects of the sea clutter radar images analysis: Nieto Borge and Guedes Soares (2000) for example proposed an approach considering superpositions of swell and wind sea components, that allows to derive wind waves and swell contributions to the total wave field, along with directional characteristic. There are also attempts to use images of the sea clutter revealed from X-band radars for estimating the current-depth profiles with a Eulerian approach (Campana et al., 2017), to retrieve wind speed and wind direction (Chen et al., 2015; Dankert and Horstmann, 2007; Dankert et al., 2003; Vicen-Bueno et al., 2013) and to derive surface characteristics (Senet et al., 2001).

On this basis several commercial systems such as WaMoS II (http://www.oceanwaves.de), SeaDarQ (Greenwood et al., 2018) and WaveFinder (Park et al., 2006) were developed. The most widely used system nowadays is WaMoS II (software and hardware details provided in Reichert at al., 1999) is focused on the operational monitoring of the sea state (wind waves and surface currents) and operational management of oil platforms and ships using nautical X-band radars. In combination with other sources of the data (altimetric wave radar, vessel hydrodynamic simulator) wind waves estimates from navigational radar can be used managing security of the offshore systems, assessing ship fatigue due to mechanical environmental influence (Drouet et al., 2013) or for the real-time prediction of ship rolling (Hilmer and Thornhill, 2015).

Natalia 26.6.2022 13:16
Удалено: The methodology of the navigational marine radar adaptation for measurements of the wind waves characteristics was announced by (Young et al., 1985). The r…adar images of t ... [2]

Natalia 26.6.2022 13:25
Удалено: the …his basis of these studies a ... [3]

We present the design and pre-proccesing methodology of the SeaVision system along with the dataset collected during three research cruises (Fig. 1). SeaVision was developed in collaboration between the Shirshov Institute of Oceanology of the Russian Academy of Sciences (IORAS, https://ocean.ru/) and the Joint stock company "Marine Complexes and Systems" ("MC&S" J.S.C., https://www.mcs.ru/). SeaVision is developed in the basis of the sea ice monitoring system with navigational marine radar – IceVision (https://ice.vision/en). The pilot version of SeaVision was tested and validated in two North Atlantic cruises in 2020 and 2021 and in the Arctic cruise in 2021 (Fig. 1). The major advantage of the presented dataset is the provision of the co-located Spotter wave buoy data with SeaVision records at almost 50 locations and outputs of WaveWatch III (WW3) model experiments forced by ERA5 reanalysis (Hersbach et al., 2020) for the corresponding domains. We present in this study the SeaVision system and dataset of the measurements of the wind waves in the open ocean and its comprehensive analysis.

The paper is organized as follows. In the Section 2 we provide details of research cruises, technical specifications of the SeaVision system, data collection and analysis principles as well as the description of the WW3 model setup. Section 3 presents the results of the analysis and validation of the SeaVision dataset against Spotter buoy data and comparison with WW3 model output. The concluding section 4 summarizes the results and discusses the perspectives of the use of ship navigation radars for a massively enhanced collection of wind wave information in the open ocean.

2 Data collection and analysis

We provide definition of all parameters in the published dataset in Appendix C.

2.1 Ship cruises

Natalia 26.6.2022 13:40
Удалено: ... [4]

Microsoft Office User 8.6.2022 16:24
Удалено: principles

Natalia 26.6.2022 13:42
Удалено: **Expeditions**

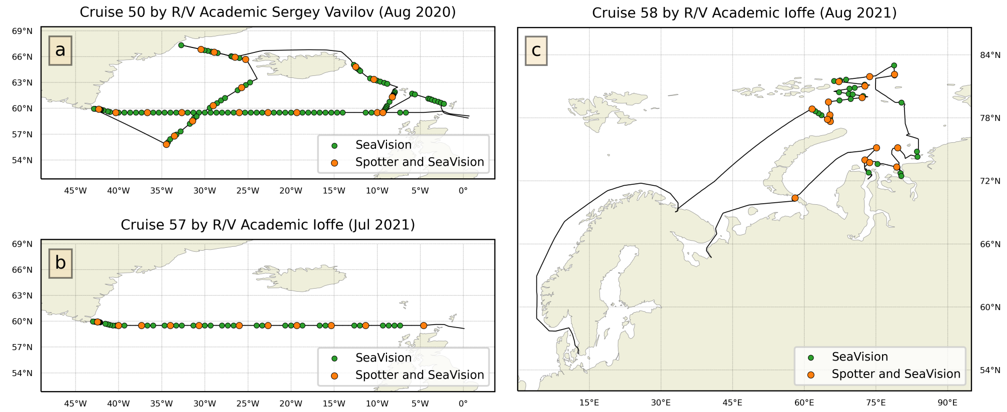

Figure 1: Ship tracks of the three cruises of the research vessels (R/V) *Akademik Sergey Vavilov* (a) and *Akademik Ioffe* (b,c). Green dots indicate locations where only SeaVision radar data were collected, orange dots show the locations for which SeaVision records were co-located with Spotter wave buoy measurements. Cruise numbers are counted from the beginnig of the R/V operation.

Figure 1 demonstrates ship tracks of three research cruises, during which wind wave data were collected. Research cruises were carried out by IORAS research vessels (R/Vs) *“Academik Sergey Vavilov”* and *“Academik Ioffe”*. Table 1 provides a general information about the cruises and detailed information on the coordinates and dates and is provided in Appendix A. The two cruises in the subpolar North Atlantic (Figure 1a, b) were focused on the regular survey of the 59.5°N oceanographic cross-section and cross-sections in the Denmark Strait (Verezemskaya et al., 2021). During these cruises the R/V makes full-depth CTD profiling. The distances between the hydrographic stations vary from ~30 km in the open ocean to a few km near the East Greenland coast with time allocated for each station (ship is drifting) varying from 2 to 6 hours. Between the stations the R/V travels at a speed of approximately 6 to 10 kn. During the cruise of R/V *“Academik Ioffe”* in the Kara Sea (Figure 1c) stations were somewhat shorter in time (2-3 hours). During all cruises wave observations were carried out after completing hydrographic profiling. For operating solely SeaVision the R/V position was strictly stationary being controlled by bow and stern thrusters of the R/V. When SeaVision was used together with the free drifting Spotter buoy, the thrusters were off to provide also free drifting of the R/V. This allowed for measurements of the background wave field by both SeaVision and Spotter buoy. At each station we first released the Spotter buoy with a supplementary floating buoy dumping cable vibrations. Such design allows for maintenance of at least 300 m distance between the buoys and the R/V. Next, both buoys were in the free-floating mode for at least 30 min during which the recording was performed by both

Natalia 26.6.2022 13:43
Удалено: **Pathways and dates**

Natalia 26.6.2022 13:42
Удалено: ***c***

Natalia 26.6.2022 13:44
Удалено: **was**

Natalia 26.6.2022 13:44
Удалено: **dots correspond to**

Natalia 26.6.2022 13:44
Удалено: **simultaneous wind waves observations**

Natalia 26.6.2022 13:44
Удалено: **and SeaVision**

Natalia 26.6.2022 13:46
Удалено: **ing**

Natalia 26.6.2022 13:48
Удалено: pathways

Natalia 14.6.2022 17:09
Удалено: and dates

Natalia 26.6.2022 13:48
Удалено: where the

Microsoft Office User 8.6.2022 16:37
Удалено: s

Natalia 17.6.2022 17:56
Удалено: along with other regular deep ocean observations. All three cruises were carried out by Shirshov Institute of Oceanology of the Russian Academy of Sciences (IO RAS) within the governmental program of regular ocean observations. In particular, two cruises in the North Atlantic (Figure 1a,b) are related to regular deep ocean observations at the 59.,5°N (Verezemskaya et al., 2021; Falina et al. 2007; Gladyshev et al. 2018, 2019; Sarafanov et al. 2008, 2018) and the Arctic expedition is a part of the IO RAS “Floating University of IORAS” program (Stepanova, 2018). In addition to the regular deep ocean observations in these cruises we were collectingcollected data from navigational radar with the newly developed SeaVision system and simultaneously carrying out observations with Spotter buoy (https://www.sofarocean.com/products/spotter). During At all “stations” research vessels were driftingdrifted during wave data collection (from 30 minutes to 2 hours) with its engines in neutral position to provide conditions for Spotter buoy wave observations in the free floating mode.

SeaVision and the Spotter buoy (Figure 4, top panel). Then both buoys were pulled back onboard. The Spotter buoy measured vertical and horizontal displacements starting from its release until getting back onboard. After completing measurements at each station only the data recorded during the free-floating mode were used for the joint analysis of SeaVision and Spotter buoy records. During all SeaVision and Spotter buoy measurements standard meteorological parameters were measured using onboard the meteostation.

Table 1: Research cruises during which wind waves observations were carried out by R/Vs *"Akademik Sergey Vavilov"* (ASV) and *"Academik Ioffe"* (AI). Adjacent numbers in the first column correspond to the R/V cruise numbers counted from the beginnig of the R/V operation.

Cruise	Start date and location	End date and location	Distance sailed	Number of stations (with Spotter buoy)
ASV50	08/08/2020 Kaliningrad Russia	08/09/2020 Kaliningrad Russia	10465 km	21
AI57	27/06/2021 Kaliningrad Russia	02/08/2021 Kaliningrad Russia	7745 km	11
AI58	08/08/2021 Arkhangelsk Russia	06/09/2021 Kaliningrad Russia	10611 km	16

2.2 SeaVision system

2.2.1 Ship navigation radar signal retrieval and preprocessing

Development of the SeaVision system was based on a commonly accepted approach of the recording and analysis of the sea clutter images. Using a similar approach to commercial systems such as WaMoS II (http://www.oceanwaves.de), SeaDarQ (Greenwood et al., 2018) and WaveFinder (Park et al., 2006) were developed. These commercial systems provide customers with their original software and hardware (sometimes including the X-band radar itself). In our approach we are focused on the development of an independently operating and low cost system compatible with the existing navigation radars with which ships are already equipped.

Research vessels *Academik Sergey Vavilov* (r/v *ASV*) and *Akademik Ioffe* (r/v *AI*) are equipped with the standard navigation X-band radar JRC JMA-9110-6XA and JMA-9122-6XA. Technical details of radar transmission and backscatter characteristics are given in Table 2. Both radars operate at 9.41 GHz frequency (wavelength ~3 cm), and are equipped with a 6 feet antenna with the directional horizontal resolution of 1.2° (Table 2). Radars can optionally operate at the pulse lengths of 0.08 µs, 0.25 µs, 0.5 µs, 0.8 µs, 1.0 µs. For our purposes we used the smallest possible pulse length of 0.08 µs (at the so-called "short-pulse" mode - SP1) providing the highest possible resolution of the image (thus the best resolution of the ocean surface). Our X-band radars are characterized by a 3.18 cm wave length of the emitted electromagnetic waves (Table 2). The pulse length is the emission time of the wave beam, thus the number of the emitted waves and the area of the reflection at the ocean surface (defining spatial resolution) increase with increasing pulse length.

The SeaVision system (Fig. 2) is connected to the radar via splitter. It provides digitizations and further recording of the directionally stabilized (northward) radar sea clutter image resulting from each single full turn of the radar antenna. By doing this, SeaVision converts the sea clutter image into a digital format with further recording the data onto the external storage. SeaVision is also connected to the ship navigation package and simultaneously records geographical coordinates from GPS, speed over ground (SOG) and course over ground (COG). Each full turn of antenna results in ASCII file (~16 MB) consisting of the 4096x4096 matrix (1.875 m discretization at 4096 beam directions) representing the sea clutter digitized image with GPS information, SOG and COG in the file header. These files are further consolidated and converted into NetCDF format at the post-processing stage.

Table 2: JRC JMA-9110-6XA radar (*R/V ASV*) and JMA-9122-6XA (*R/V AI*) transmission and reception characteristics.

Research vessel	*Akademik Sergey Vavilov*	*Akademik Ioffe*
Radar type	JRC JMA-9110-6XA	JMA-9122-6XA
Radar frequency/Wave length	9.41 GHz / 3.18 cm	9.41 GHz / 3.18 cm
Antenna rotation speed	27 rpm	24 rpm
Impulse power	10 kW	25 kW
Antenna size	6 ft	6 ft
Pulse length mode	0.08 µs (short pulse)	0.07 µs (short pulse)
Analog-digital converter (ADC) frequency/size of output matrix for one antenna turn	80 MHz / 4096x4096	80 MHz / 4096x4096
Azimuthal coverage/resolution	0 – 360°/1.2°	0 – 360°/1.2°
Distance range	231.5 – 2778 m	231.5 – 2778 m

Natalia 20.6.2022 16:06
Удалено: ... [5]

Natalia 21.6.2022 14:43
Удалено: For our purposes we used the shortest possible pulse length of 0.08 µs (at so-called “short-pulse” mode - SP1), that is equivalent to a 12 m angular spatial resolution.

Natalia 26.6.2022 14:19
Удалено: , it digitizes and records directionally stabilized (northward) radar sea clutter images (converted to netcdf format during postprocessing) of each radar antenna rotation in digital format to the external storage, it is also connected to the ship’s navigational equipment and records parameters such as: GPS geographical coordinates, speed of the ground (SOG), course of the ground (COG)

Natalia 26.6.2022 14:21
Удалено: turn

Natalia 26.6.2022 14:21
Удалено: a separate

Natalia 26.6.2022 14:21
Удалено: with the

Microsoft Office User 8.6.2022 16:19
Удалено: h

Microsoft Office User 8.6.2022 16:19
Удалено: h

Microsoft Office User 8.6.2022 16:25
Удалено: ,

Microsoft Office User 8.6.2022 16:25
Удалено: ,

Range resolution	12 m	10.5 m
Analog-digital converter (ADC) frequency/size of output matrix for one antenna turn	80 MHz / 4096x4096	80 MHz / 4096x4096
Calibration coefficients A and B	A = -0.4042, B = 1.0034	A = -0.4042, B = 1.0034

Microsoft Office User 8.6.2022 16:19
Удалено: h

Microsoft Office User 8.6.2022 16:20
Удалено: h

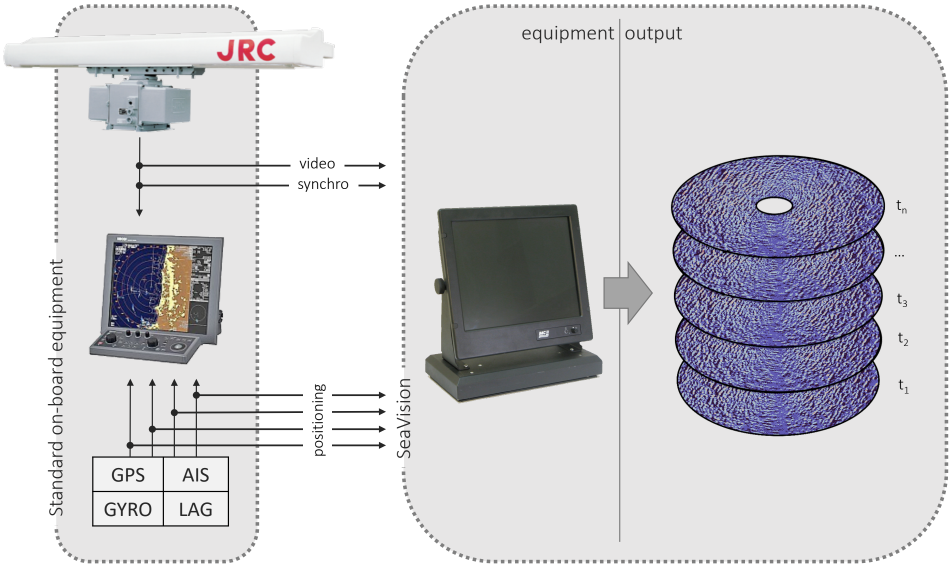

Figure 2: SeaVision integration to the ship's navigational equipment together with an example of the series of the geographically stabilized (northward) sea clutter images, one for each antenna turn (right column). Image of the JRC radar scanner (top left) is taken from the http://www.jrc.co.jp/eng/index.html.

Natalia 26.6.2022 14:24
Удалено: est

Natalia 26.6.2022 14:24
Удалено: tor

Natalia 27.6.2022 21:47
Удалено: www.jrc.co.jp.

2.2.2 Analysis of the sea clutter images

After the sea clutter images are collected and digitized, the next step is the postprocessing focused on the computation of significant wave height (H_s), wave period (T_{m1}), wave energy spectrum (S_w) and wave direction (D_s). Here we provide a short condensed description of the algorithm with the full details given in Appendix B. The subset collected at each station (Fig. 1) consists of 20 minutes SeaVision record, which is equivalent to at least 540 images of the sea clutter (27 antenna full turns per minute for JRC JMA-9110-6XA radar).

The methodology for estimation of wind wave characteristics relies on a a well established Fourier Transform (FT) technique (Nieto-Borge and Guedes Soares, 2000; Borge et al., 2004, Borge et al., 2008 among others). For each station preprocessing of the data begins from the choice of the processing squared area (squared area of 720×720 m). For now we locate the processing area visually by taking the area of the most apparent wave signal at the image and requiring this area to be deviated from the ship by 300 m to avoid a potential impact of the ship on the wave field and the effects of the reflection and modulation of the radar signal by the ship superstructure. When the processing area is selected, we consolidate the data captured in this area from all 540 images for the further analysis. Note that data initially sampled in the polar coordinates are re-gridded at this step to the Cartesian grid of 384x384 grid points with 1.875 m spatial resolution for each subset.

The sequence of 540 matrixes with 384×384 grid points each is then split into 16 sectors (22.5^o width each). Further, to obtain the directional spectra estimates, we transformed the data into a 3D spectral domain by using FT and applying the Welsh method with a half-width overlapping Hanning window (Fig. 3). This returns for each sector the three-dimensional spectrum $S_{3d,image}(k_x, k_y, f)$, where $f = \omega/2\pi$ is the frequency (Hz) and ω is the angular frequency, k_x and k_y (rad/m) are the components of the wave vector $\vec{k}(k_x, k_y)$. Then for each sector we capture the spectrum power within the band along the line satisfying the linear dispersion relation for ocean waves (Fig. 3):

$$\omega = \sqrt{gk} + kUcos\theta\ , \tag{1}$$

where k is the wave number (rad/m), g is gravity (m/s^2), U is the surface velocity (m/s) which includes surface current velocity and ship drift, and θ is the angle between the wave vector $\vec{k}$ and velocity vector $\vec{U}$. This procedure is applied to the bands corresponding to the first and the second spectral harmonics (see Appendix B for the definition of band width). The spectral power outside the bands for the two harmonics is assumed to be a background speckle-noise ($\omega_{speckle}$) (Kanevsky, 2008). Integrated spectral power outside of the bands matching the wave dispersion relation (1) is further used for estimation of the signal-to-noise ratio (SNR) as described in Appendix B and outlined in many works (Nieto-Borge et al., 1999; Hessner et al., 2002; Young et al 1985, Nieto-Borge and Guedes Soares 2000, Ivonin et al. 2016). Following Nieto-Borge et al. (1999, 2004) SNR is then converted to significant wave height $H_{s,SeaVision}$ using the linear regression equation:

$$H_{s,SeaVision} = A + B\sqrt{SNR}, \tag{2}$$

Natalia 26.6.2022 14:25
Удалено:

Natalia 26.6.2022 14:25
Удалено: ... [6]

Natalia 26.6.2022 14:37
Удалено: long observations with

Natalia 26.6.2022 14:37
Удалено: it

Natalia 26.6.2022 14:37
Удалено: minimum

Natalia 26.6.2022 14:41
Удалено: at one station

Natalia 26.6.2022 14:41
Удалено: M

Natalia 26.6.2022 14:42
Удалено: s'

Natalia 26.6.2022 14:42
Удалено: estimates

Natalia 26.6.2022 14:42
Удалено: is

Natalia 22.6.2022 11:32
Удалено: Fast

Natalia 26.6.2022 14:42
Удалено: based

Natalia 26.6.2022 14:43
Удалено: (with a side of 720 m)

Natalia 26.6.2022 14:43
Удалено: At this stage we locate the processing area by visual choice of the most apparent wave signal on the images and minimal distance from the ship of 300 m (to avoid potential impact of the ship to the wave field and illumination of the radar signal by the ship). After choosing the area we create the dataset for the further analysis by sampling the same squares from each image (one antenna turn). Data sampled in the polar coordinates were regridded to the Cartesian grid resulting in 384x384 pixels dataset array (with 1.875 m spatial resolution) for each station.

Natalia 26.6.2022 14:44
Удалено: The sequence of these images is then transformed to the 3D spectral domain using fast Fourier transform (FFT, Fig. 3)

where A and B are empirical calibration coefficients which are individual for each radar. In this study these coefficients were computed by fitting a linear regression (2) to the significant wave height measured by the Spotter wave buoy. Derived numerical values of A and B coefficients are given in Table 2 for both X-band radars. Wave period $T_{m01,SeaVision}$ was estimated conventionally using zeroth and first spectral moments:

$$\mathrm{m}_{1,\mathrm{SeaVision}} = \int_0^\infty S_{w,SeaVision}(f)df \tag{3}$$

$$T_{m01,SeaVision} = \frac{m_0}{m_1}, \tag{4}$$

where $S_{w,SeaVision}(f)$ is the estimate of the wave energy spectrum from SeaVision:

$$S_{w,SeaVision}(f) = \left(\frac{\mathrm{H}_{\mathrm{s,SeaVision}}}{\mathrm{H}_{\mathrm{s,image}}}\right)^2 \mathrm{S}_{\mathrm{image}}(f) \tag{5}$$

(4)

$$T_{m01,SeaVision} = \frac{m_0}{m_1} \tag{5}$$

where $S_{w,SeaVision}$ is the estimate of the wave energy spectrum from SeaVision:

$$S_{w,SeaVision}(f) = \left(\frac{\mathrm{H}_{\mathrm{s,SeaVision}}}{\mathrm{H}_{\mathrm{s,image}}}\right)^2 \mathrm{S}_{\mathrm{image}}(f) \tag{6}$$

where $H_{s,image}$ is $H_{s,image} = 4\sqrt{m_{0,image}}$, thus being the estimate of significant wave height using the raw sea clutter image before calibration.

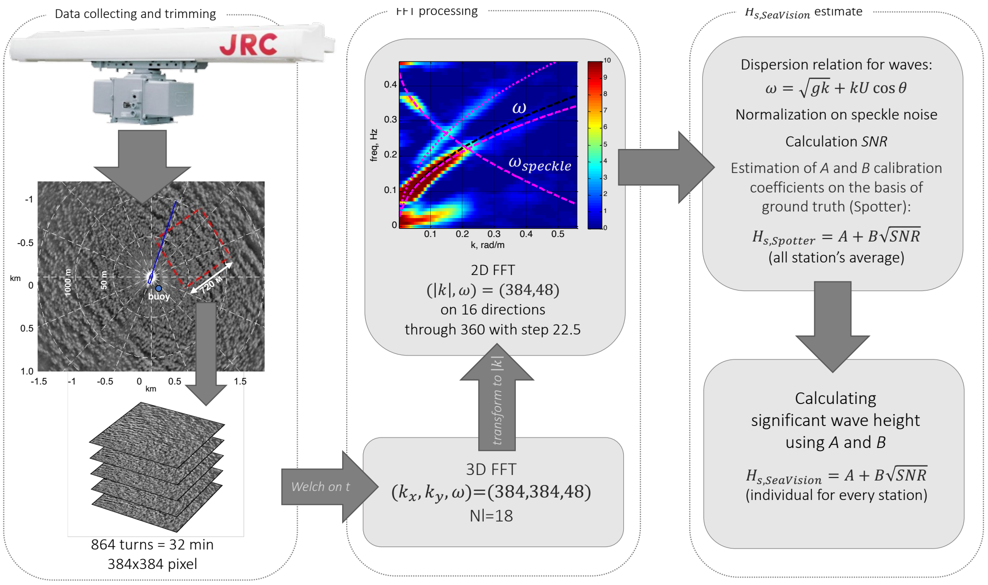

Figure 3: Organigram of the data processing for estimation of wind waves parameters from the sea clutter images. JRC radar scanner (top left) is taken from the http://www.jrc.co.jp/eng/index.html.

2.3 Spotter wave buoy data

To calibrate and validate SeaVision wave observations we performed simultaneous measurements with the Spotter wave buoy (https://www.sofarocean.com/products/spotter) in the locations shown in Figure 1 and specified in Table A1. Once the ship is drifting at the location of the measurements, the Spotter buoy was deployed and started move away from the ship. Note that the ship drift is always faster compared to that of the buoy, thus the distance between the buoy and the ship was progressively increasing. When the distance between the ship and the buoy reached at least 300 m, the "free floating" mode of SeaVision and Spotter buoy operation was initiated for at least 30 minutes as described in section 2.1. The longest free floating mode time period at some stations reached up to 1.5 hours. To ensure homogeneity of the analysis we used 20-minute segments from "free floating" mode time series for further computations of significant wave height, wave spectra and directional moments following Raghukumar et al. (2019): $H_s = 4\sqrt{E}$, where $E = \int_{0.01\,Hz}^{1.25\,Hz} E(f)df$ - the surface elevations

Natalia 26.6.2022 15:15
Удалено: Data processing schematic for estimation of the wind waves parameters from the sea clutter images. Image of the

Natalia 26.6.2022 15:15
Удалено: tor

Natalia 27.6.2022 21:47
Удалено: **www.jrc.co.jp.**

Microsoft Office User 7.6.2022 18:26
Удалено: s

Natalia 26.6.2022 15:20
Удалено: a series of

Natalia 26.6.2022 15:20
Удалено: of the wave parameters with

Natalia 26.6.2022 15:21
Удалено: demonstrates the track of the three cruises indicating locations where wind waves were measured simultaneously with Spotter wave buoy and SeaVision, Table A1 provides a list of all locations where SeaVision+Spotter buoy (or SeaVision only) measurements were carried out.

Natalia 26.6.2022 15:21
Удалено: was in a

Natalia 26.6.2022 15:21
Удалено: drift

Natalia 26.6.2022 15:22
Удалено: according to the plan of the cruise, the

Natalia 26.6.2022 15:22
Удалено: equipped, sent overboard and allowed to

Natalia 26.6.2022 15:22
Удалено: for at least 200 m (as the ship drift is faster than buoy drift due to the local winds, the distance between buoy and ship was constantly increasing). Starting from at least 200 m separation the buoy was in a "free floating" mode recording horizontal and vertical displacements of itself. For each station we allowed for at least 20 minutes of the free floating buoy measurements, however at some stations this was up to 1.5 hours.

Natalia 26.6.2022 15:24
Удалено: For the homogeneity of the analysis for all stations we used 20-minute time series for wave parameters calculation. ... [7]

Natalia 27.6.2022 21:42
Удалено: 0.01

Natalia 27.6.2022 21:42
Удалено: 0.

Natalia 27.6.2022 21:42
Удалено: 3

variance in the frequency range of the wind waves. Further use wave parameters derived from the Spotter buoy as a "ground truth" for the calibration of SeaVision data and derivation of A and B calibration coefficients in (2) (Table 2).

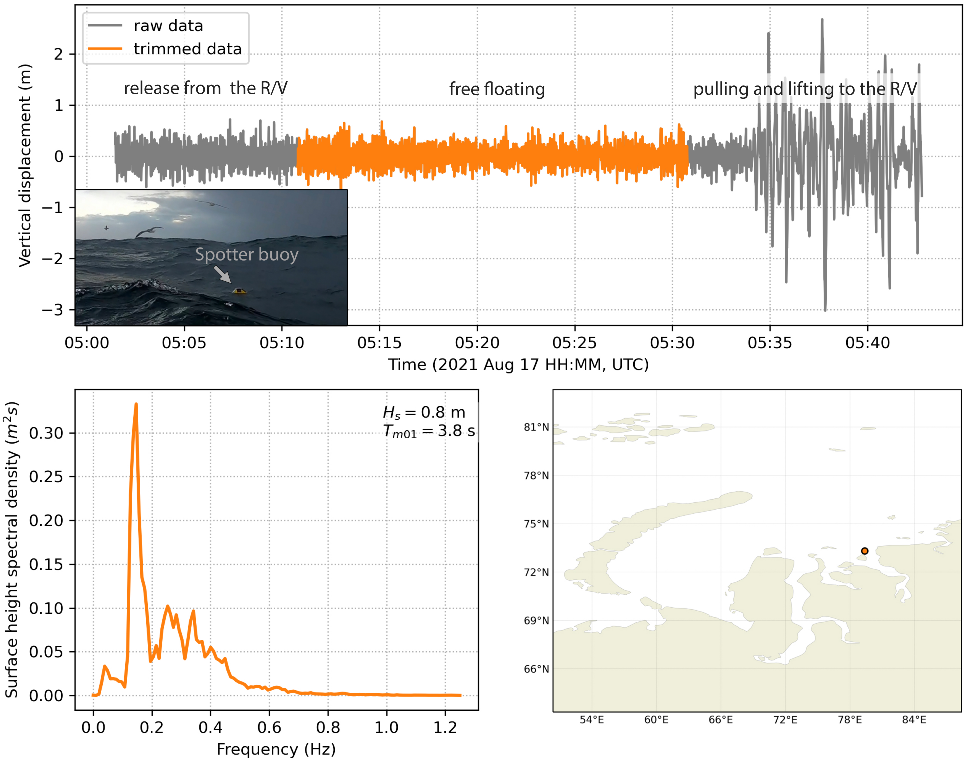

Figure 4: Spotter wave buoy timeseries of vertical displacements at the station #3946 in the AI58 cruise (a), corresponding wave energy spectrum (b) and location of the station #3946 (c).

2.4 Meteorological data

During all cruises the AIRMAR WeatherStation 220WX was installed on the main ship mast at 30 m height above the sea. The weather station provided an output consisting of standard output parameters (barometric pressure, wind speed and direction, air temperature and relative humidity). Wind characteristics were recalculated from the relative wind to the true wind in real-time mode.

Natalia 26.6.2022 15:25

Удалено: More details on calculation of the mean wave direction, directional spread, wave directional spectrum and other parameters on the basis of the Spotter time series can be found in (Raghukumar et al., 2019), together with evaluation of the buoy ability for wave characteristics measurements ... [8]

Natalia 26.6.2022 15:25

Удалено: from

Natalia 26.6.2022 15:25

Удалено: buoy as the

Natalia 26.6.2022 15:26

Удалено: calibration and estimation of the radar calibration coefficients *A* and *B*, these coefficients are further used to rescale SeaVision wave energy spectrum to match buoy spectrum with least squares.

Natalia 26.6.2022 15:28

Удалено: th

Natalia 26.6.2022 15:29

Удалено: of R/V *Academic Ioffe*

Natalia 27.6.2022 21:43

Удалено: top

Natalia 26.6.2022 15:29

Удалено: together with significant wave height

Natalia 27.6.2022 21:43

Удалено: bottom left

Natalia 26.6.2022 15:30

Удалено: directional wave spectrum (bottom right)

Natalia 26.6.2022 15:30

Удалено: Along

Natalia 26.6.2022 15:31

Удалено: mounted at the height of 30 m

Natalia 26.6.2022 15:31

Удалено: to avoid the impact of the ship on the local meteorology. W

Natalia 26.6.2022 15:31

Удалено: provides

Natalia 26.6.2022 15:31

Удалено: standard

2.5 WaveWatch III model experiment

We run WaveWatch III (WW3DG, version 6.07, WW3) spectral wave model forced by ERA5 reanalysis (Hersbach et al., 2020) over the domain and the time period of the research cruises (Table 3). The experiments were performed for the outer domain at 0.1° spatial and 1-hr temporal resolution and for the inner domain with 0.03° (~1 km) resolution (see Table 3). The outer domain solution was used for setting lateral boundary conditions for the inner domain. These experiments returned two - dimensional wave spectra co-located with SeaVision and Spotter buoy observations. In the WW3 experiments we used the ST6 parameterization (Babanin, 2006; Babanin, 2011; Rogers et al., 2012; Zieger et al., 2015) for wave energy input and dissipation and the discrete interaction approximation (DIA) scheme for nonlinear wave interactions (Hasselmann and Hasselmann 1985). This WW3 setting is close to that used in Sharmar et al. (2021) for the global wind wave hindcasting.

Table 3: WW3 model configuration over the domains of expeditions.

Cruise	ASV50	AI57	AI58
Region	North Atlantic polygon	North Atlantic polygon	Arctic polygon
Grid type	Regular, nested grid	Regular, nested grid	Curvilinear grid
Outer domain spatial resolution	30°-75°N and 80W-10E 0.1°x0.1°	30°-75°N and 80W-10E 0.1°x0.1°	36°-90°N and 0°-360° 0.1°x0.1°
Inner domain spatial resolution	54°-68°N and 45°W-1°E 0.03°x0.03°	54°-68°N and 45°W-1°E 0.03°x0.03°	-
Time coverage	2020.08.01-2020.09.06	2021.06.01-2021.07.12	2021.08.01-2021.09.30

3 Results of validation of SeaVision measurements

Validation of SeaVision data was provided for wind speeds from 2 to approximately 20 m/s^{-1} and for significant wave heights from few tens of centimeters to 4.2 meters. Figure 5 demonstrates the results of the intercomparison of significant wave height (H_s) estimates retrieved from SeaVision data and those measured by Spotter buoy and simulated with WaveWatch III. The H_s differences 'Spotter minus SeaVision' (Fig. 5a) and 'WW3 minus SeaVision' (Fig, 5b) are plotted as a function of wind speed recorded by the ship weather station (Table A1). Table 4 provides comparative estimates of differences in H_s for the three cruises. On average WW3 yields lower wave heights than SeaVision H_s by 28 cm, while the agreement between SeaVision and Spotter buoy data is better with H_s measured by Spotter being 9 cm higher than retrieved from SeaVision. For low wind speeds SeaVision tends to underestimate H_s up to 50 cm and for moderate and strong winds

Natalia 26.6.2022 15:32

Удалено: parameters: barometric pressure, wind speed and direction, air temperature and relative humidity. Wind characteristics were recalculated from apparent wind to true wind in real-time.

Microsoft Office User 8.6.2022 16:29

Удалено:

Natalia 26.6.2022 15:32

Удалено: Another potential source of the wind waves data in the open ocean is spectral wave modelling.

Natalia 26.6.2022 15:32

Удалено: with

Natalia 26.6.2022 15:33

Удалено: as lateral boundary conditions with 0.1° spatial and 1 hourly temporal resolutions

Natalia 26.6.2022 15:34

Удалено: The experiments have been developed to reconstruct two- dimensional wave spectra comparable with SeaVision and Spotter buoy observations. Start and end dates of the experiments were collocated in time with dates of the research cruises. For wave energy input and dissipation we use ST6 parameterization (Babanin, 2006; Babanin, 2011; Rogers et al., 2012; Zieger et al., 2015) and the discrete interaction approximation (DIA) scheme for nonlinear wave interactions (Hasselmann and Hasselmann 1985).

Natalia 26.6.2022 15:34

Удалено: **Validation and overall SeaVision performance**

Microsoft Office User 25.6.2022 3:10

Удалено: for all data collected

Natalia 24.6.2022 20:14

Удалено:
tendency to e the $H_s$by On average WW3
WW3 underestimates H_s by 27 cm, while SeaVision on average implies agreement with Spotter buoy data – only 3 cm on average on average. In general, for the lower wind speeds SeaVision underestimates H_s by up to 50 cm and somewhat overestimates H_s for the higher wind speeds. This effect can be due to better ripples development on the ocean surface during higher winds affecting the signal to noise ratio (Formula 1).

the analysis shows an overestimation of SeaVision H_s compared to buoy and model data. This can be explained by better developed ripples (affecting the signal to noise ratio) at the ocean surface under stronger winds.

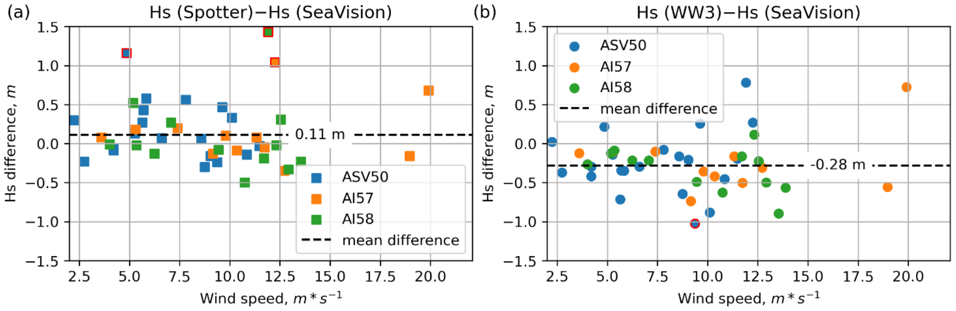

Figure 5: Difference in the significant wave height (H_s) estimates for all stations as a function of the wind speed: Spotter buoy ("ground truth") *minus* SeaVision (a), WW3 *minus* SeaVision (b). Dash lines mark the mean difference across all data points. Red squares and circles mark differences higher than 1 m.

We also identified two locations (2901 and 2937, see Table A1) for which the differences between the Spotter buoy data and SeaVision reach more than 1 m (for 5 and 13 m/s winds). Weather conditions for these two cases were not associated with severe weather and H_s values were in the range between 1.5 and 2 m. However, in both cases we recorded a strong drift of the vessel due to the local current that potentially impacted the angle of the electromagnetic signal reflection from the surface and hence affected the accuracy of the radar images. Thus, strong ship drift may influence the SeaVision results and the data collected under strong ship drift should be considered with caution. These cases, in the future, can be identified by analysis of speed over ground (SOG parameter).

Table 4: Differences in significant wave height estimates for three cruises.

Mean difference in H_s (m)	ASV50	AI57	AI58
Spotter - SeaVision	0.27	0.05	-0.06
WW3 - SeaVision	-0.24	-0.24	-0.36

Scatterplots for the H_s and wave period (T_{m01}) demonstrate generally a better agreement between different data sources for H_s (1.06 and 1.02 regression coefficients) than for T_{m01} (1.05 and 0.86 regression coefficients) (Fig. 6). There is no robust evidence of the dependence of the magnitude or sign of H_s and T_{m01} differences on the magnitude of parameters themselves. We also note that both SeaVision and Spotter show higher waves and slightly longer periods compared to WW3 (Fig. 6). We

Natalia 26.6.2022 15:38

Удалено: tendency to e the $H_s$by On average WW3 underestimates H_s by 27 cm, while SeaVision on average implies agreement with Spotter buoy data – only 3 cm on average on average. In general, for the lower wind speeds SeaVision underestimates H_s by up to 50 cm and somewhat overestimates H_s for the higher wind speeds. This effect can be due to better ripples development on the ocean surface during higher winds affecting the signal to noise ratio (Formula 1).

Natalia 22.6.2022 17:51

Удалено: left panel…), WW3 *minus* Sea ... [9]

Natalia 24.6.2022 20:30

Удалено: At the same time there are two stations (2901 and 2937 see Table A1) where this difference reaches almost 100 cm (between 59 and 132 m/s winds), examinations of weather conditions at these stations revealed that there were not any special weather conditions and observations were carried for H_s between 1.5 and 2 m, however there was a strong drift of the vessel due to the local current that potentially influenced the angles of electromagnetic signal reflection from the surface and hence affected the accuracy of the radar images. For the cases of the strong drift of the vessel and other non-standard situations in the open ocean we will collect more data and investigate into these differences. In Table 4 we provide average differences of H_s for three expeditions.

Natalia 27.6.2022 21:46

Удалено: Table 4: Differences in significant wave height estimates for three expeditions.
ASV50 ... [10]

Microsoft Office User 8.6.2022 16:07

Удалено: Further examination and methodology adjustment required together with more data collection during different conditions in the open ocean are required to investigate into these differences.

Microsoft Office User 23.6.2022 1:24

Удалено: $_s$… also ... [11]

Natalia 24.6.2022 20:39

Удалено: s

Microsoft Office User 23.6.2022 1:35

Удалено: b…1.05 and 0.86 regression ... [12]

Natalia 24.6.2022 20:41

Удалено: also…no evident dependance f ... [13]

Microsoft Office User 25.6.2022 3:23

Удалено: biases…ifferences on the magn ... [14]

note however, that simulated wind waves with WW3 strongly depend on the atmospheric forcing (choice of reanalysis). Difference in climatological mean values over the North Atlantic obtained with WW3 but with different forcing functions can reach few tens of centimeters (Sharmar et al. 2021).

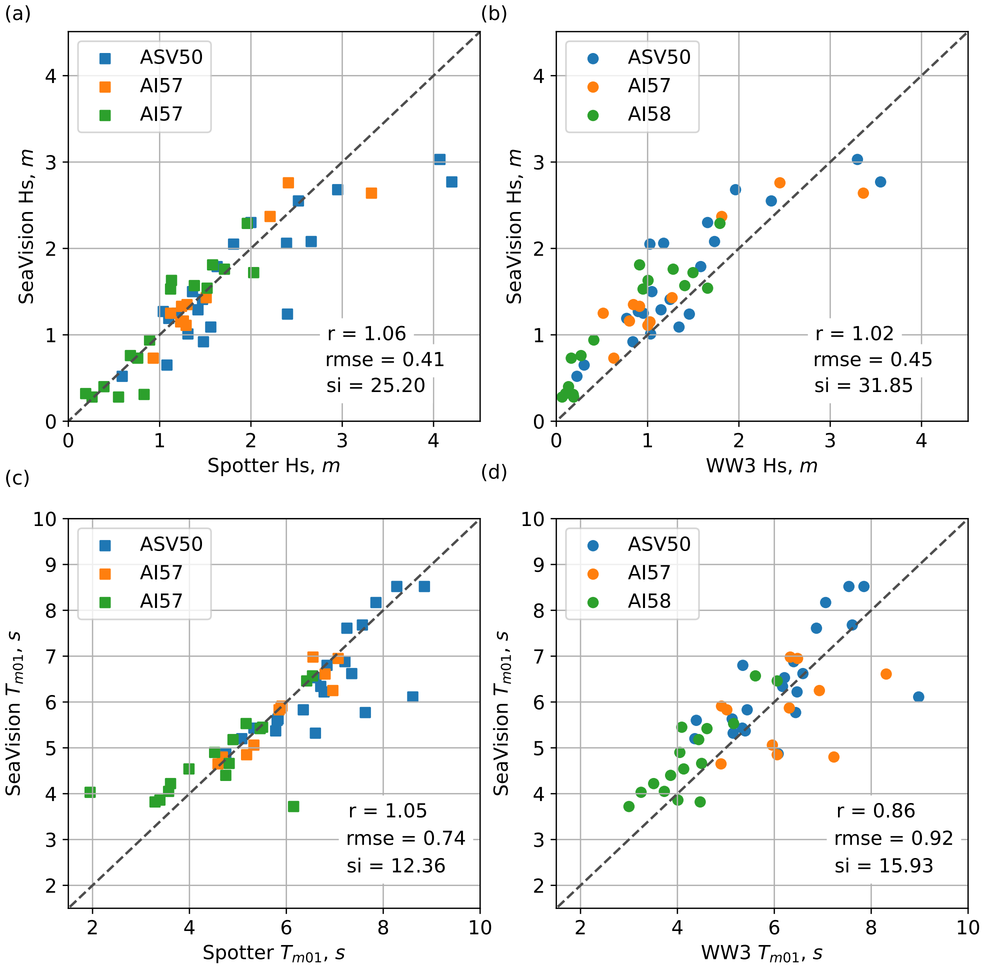

Figure 6: Scatterplots of the significant wave height (H_s) and wave period (T_{m01}) revealed by SeaVision and measured by Spotter (a,c) as well as revealed by SeaVision and simulated with WW3 (b,d) for all stations.

Natalia 26.6.2022 15:41
Удалено: should

Natalia 26.6.2022 15:41
Удалено: reanalysis

Microsoft Office User 25.6.2022 3:26
Удалено: and in the subpolar North Atlantic climatological mean values

Microsoft Office User 25.6.2022 3:26
Удалено: taken from different reanalyses can differ from each other by

Microsoft Office User 23.6.2022 1:23
Удалено: ,

Natalia 24.6.2022 20:44
Удалено: estimates between

Natalia 24.6.2022 20:44
Удалено: and between

Overall, the analysis of significant wave heights among these three sources of data (Spotter, SeaVision and WW3) shows that the highest H_s values are measured by the Spotter buoy, lowest are simulated by WW3, with SeaVision being in between. These results are intuitively correct as wave buoys measure the actual elevations of ocean surface, SeaVision provides a proxy of local wave conditions from image analysis (thus imposing averaging over the domain) and is not expected to be as accurate as wave buoy data.

Figure 7 shows comparisons of wave directions along with corresponding H_s values (simplified approximation of directional spectra) for six stations (see Table A1). Generally all three data sources demonstrate very good agreement on directions (differences in waves direction do not exceed 10°) with corresponding wave height estimates being underestimated in model simulations as already mentioned above (Figures 5 and 6).

Natalia 26.6.2022 15:43
Удалено: is

Natalia 26.6.2022 15:43
Удалено: s

Natalia 26.6.2022 15:43
Удалено: SeaVison

Natalia 26.6.2022 15:44
Удалено: ries

Natalia 26.6.2022 15:44
Удалено: , WW3 underestimates H_s in local points

Natalia 24.6.2022 20:43
Удалено: Estimates of the H_s from directional spectra are shown in Figure 7 for six stations (see Table A1). It is important to notice that all three sources of the data: SeaVision, Spotter buoy and WW3 demonstrate higher agreement in estimates of the waves directions (from) than in H_s or $T_{m01}T_s$. The difference in waves direction does notdoesn't exceed 10°.

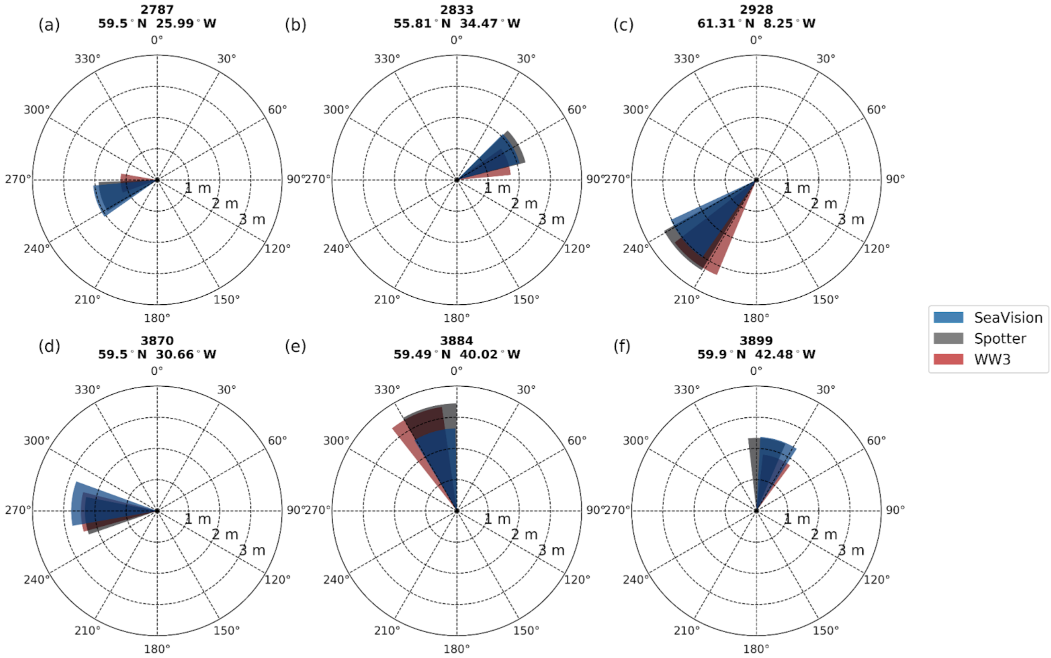

Figure 7: Diagrams (roses) of wave direction (from) and H_s on the basis of the three data sources: SeaVision (blue), Spotter (gray) and WW3 (red) at the stations: #2787, #2833, #2928, #3870, #3884, #3899 (see Table A1).

We also performed comparisons of SeaVision and Spotter H_s estimates with satellite altimeter missions (Figures 8, 9). Figure 8 shows overpasses of all available satellite tracks of Jason-3, CFOSAT, Sentinel-3A, Sentinel-3B, SARAL and HaiYang-2B which are suitable for comparisons with our dataset. Altimeter data were used for comparisons when they satisfied two conditions: an overpass was within 2° latitude and within ±30 minutes from the measurement time (Table A1). In total we selected 20 cases that satisfied these conditions.

Natalia 27.6.2022 21:43
Перемещено (вставка) [1]

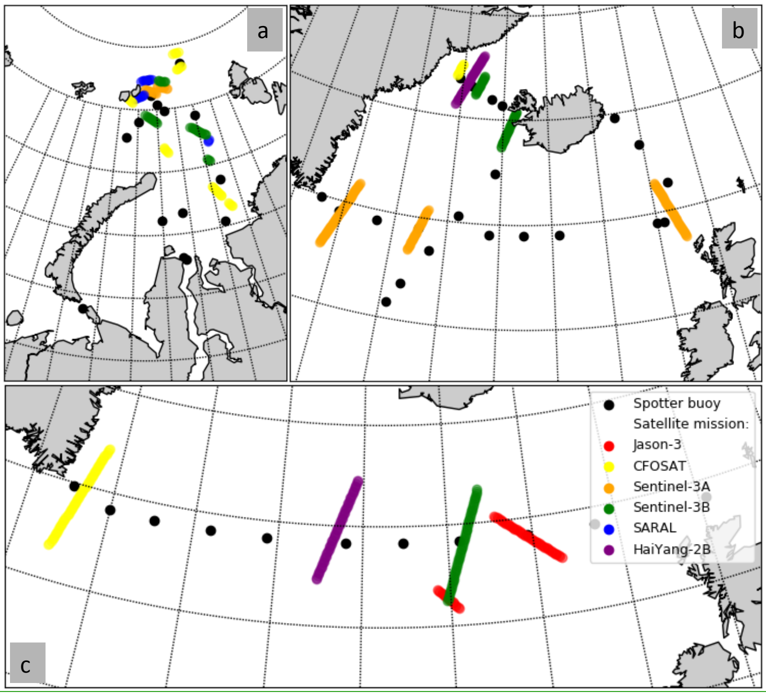

Figure 8: Overpasses of satellite altimeter missions (Jason-3, CFOSAT, Sentinel-3A, Sentinel-3B, SARAL or HaiYang-2B) over the observational domains. Black dots indicate locations where wave parameters were measured simultaneously with Spotter wave buoy and SeaVision (Table A1).

The average H_s for these 20 locations measured by satellite altimeters is 1.47 m, with Spotter buoy is 1.38 m and SeaVision giving 1.26 m. There is a general agreement for most stations among these three sources of data and differences do not exceed 50 cm except for two cases: stations 2937 and 2901, where H_s is underestimated by SeaVision comparing to Spotter and altimeter by more than 100 cm. These two outliers were already mentioned above (Figure 5) and large differences were attributed to a very strong drift of the ship for these locations.

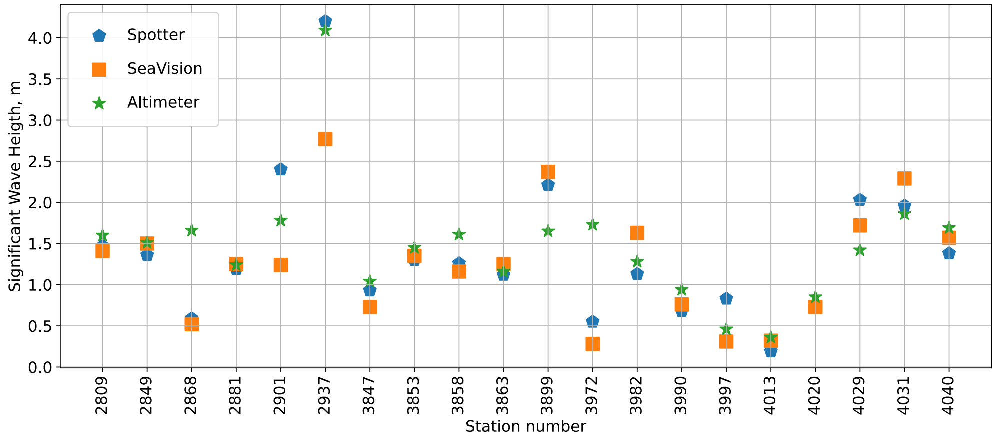

Figure 9: Significant wave height estimates for the locations of satellite altimeters overpasses for three research cruises. Numbers on the horizontal axis correspond to the station numbering in Table A1.

Conclusions

To open a new avenue for widely needed broad-scale high-quality observations of ocean wind wave estimates we used a conventional navigation X-band ship radar equipped with a SeaVision recorder and software package and here present the evaluation of the instrument package for measuring wind wave parameters and comparing them with in-situ observations and model results. The data were collected on three cruises in the subpolar North Atlantic and in the Kara Sea. All SeaVision records were co-located with in-situ Spotter buoy measurements used for validation. We demonstrate an overall agreement of the estimates of significant wave height and wave period measured by SeaVision with Spotter buoy measurements and with simulations with the WW3 spectral wave model. Estimates of significant wave height between SeaVision, WW3 and Spotter buoy are in a better agreement than those for the wave periods. In the ranges of H_S up to 4.2 m the average difference between the Spotter buoy and SeaVision is 9 cm for H_S, while WW3 simulations are higher than SeaVision H_s by 28 cm. We note, however, that comparisons with WW3 should be considered with caution, as the model results are significantly dependent on the choice of forcing function (atmospheric reanalysis). SeaVision tends to underestimate mean wave periods by ~0.5 s compared to the Spotter buoy while the differences in periods with WW3 simulations may amount to more than 2 sec. Also, a very good agreement was found for the wave directions whose spread across all three data sources does not exceed 10°.

Natalia 27.6.2022 21:43

Перемещено вверх [1]: We also performed comparisons of SeaVision and Spotter H_s estimates with satellite altimeter missions (Figures 8, 9). Figure 8 shows overpasses of all available satellite tracks of Jason-3, CFOSAT, Sentinel-3A, Sentinel-3B, SARAL and HaiYang-2B which are suitable for comparisons with our dataset. Altimeter data were used for comparisons when they satisfied two conditions: an overpass was within 2° latitude and within ±30 minutes from the measurement time (Table A1). In total we selected 20 cases that satisfied these conditions.

Natalia 26.6.2022 16:31

Отформатировано: Подстрочный

A newly developed SeaVision system for digitizing and recording of the analog signals from navigation radars and further quantitative estimation of wind wave characteristics promises to enhance massive observations of wind waves over the open ocean. SeaVision is currently mounted onboard two R/Vs operated by IORAS, but in 2022 five more IORAS R/Vs will be supplied with SeaVision systems. Data records will become operationally available at an open source web page. In 2023 we also plan to develop a portable and cheap version of SeaVision that can be easily mounted on any ship with navigational radar operating in the open ocean, on the platform, lighthouse or any coastal infrastructure. After further validation SeaVision can be easily upgraded to incorporate all post-processing procedures into the internal software package that will make it possible for commercial ships on which the system is installed to provide real-time reporting of wind wave parameters though the Global Telecommunication System (GTS). Theoretically the estimated data flow is formally one estimate per 2-3 seconds (1 full turn of the radar antenna). Even with a reporting frequency once per minute the potential of the SeaVision data flow overestimates the current VOS data flow by hundred times. Contrasting to exiting commercial systems for wind waves monitoring with navigational marine radars, such as WaMoS II (http://www.oceanwaves.de), SeaDarQ (http://www.seadarq.com/) and WaveFinder (Park et al., 2006), SeaVision is focused on the use of information of conventional navigation ship radars representing potentially a low cost alternative. Wide use of such a system at commercial ships can drastically increase the amount of sea state observations available to users, including National Meteorological Offices using this information as data assimilation input for NWP models and reanalyses.

The Global Climate Observing System (GCOS) and associated Global Ocean Observing System (GOOS) are considering sea state to be a critical climate variable highly demanded by global observing modules. We hope that SeaVision with its perspective to provide exceptionally high global coverage with on-line wave measurements will meet this urgent demand and help to satisfy GCOS given its mandate for systematic observations under the UN Framework Convention on Climate Change (UNFCCC), including also GCOS and GOOS responsibilities under the Subsidiary Body for Scientific and Technological Advice (SBSTA) and the Subsidiary Body for Implementation (SBI).

Data availability

Datasets that contains significant wave height, wave period, wave direction, wave energy frequency spectrum, meteorological data and other related parameters from both SeaVision and the Spotter buoy at the locations of every station (Table A1, Gavrikov et al., 2021) is available through the PANGAEA repository (https://doi.pangaea.de/10.1594/PANGAEA.939620). In this dataset we only provide wind waves statistics, disregarding separation of the swell and wind waves at this stage of the SeaVision development. We plan to include this procedure into the next studies. At the same time, we provide one dimensional spectrum that potentially allows to see first and seconds peaks associated with winds waves and swell (an example is shown in Figure 4b). Users interested in the analysis of the raw

Natalia 26.6.2022 15:59

Удалено: In this study we present the dataset of the observations of the wind waves collected during three research cruises (two in the North Atlantic and on in the Arctic) on the basis of usage navigational X-band marine radar and wave buoy Spotter. Nowadays there is still exists gap in the *in situ* observational network for the wind waves, at the same time Wwinds waves is are crucially important dynamical components of the interaction between the ocean and the atmosphere and play important role into the climate system, however *in situ* observational network for the wind waves is still sparse. We also present a newly developed SeaVision system for digitizing and recording of the analogous marine radar signal and further analysis of the data to obtain wind waves' parameters such as significant wave height, wave period and wave energy spectruma. The potential usage of the dataset is validation of the satellite missions and outputs from the wave models.

Natalia 26.6.2022 16:00

Удалено: We demonstrate an overall agreement of the estimates of significant wave height and wave period on the basis of SeaVision with the same estimates simultaneously measured by the wave buoy Spotter and modelled by WW3 spectral wave model. At the same time estimates of the significant wave height between WW3, Spotter and SeaVision are in a better agreement than estimates of the wave period. Within the H_s up to 4.2 m and T_s up to 10 s the average difference between SeaVision Spotter and Spotter SeaVision buoy is 3 9 cm for H_s, while for the Spotter WW3 minus WW3 SeaVision this difference is -287 cm, meaning underestimation of wave heights by WW3 comparing to SeaVision and slight (9 cm) underestimation of wave height by . SeaVision comparing to Spotter buoy. SeaVision has a tendency (relatively to Spotter) to overestimate underestimate mean period by 0.5 s while WW3 both overestimates and underestimates wave periods by up to 2.,5 s (regression coefficient with SeaVisionpotter is only 0.7663, Fig. 6). The best agreement among three sources of the data is in estimation of wave directions (Fig. 7), the difference doesn't exceed 10°. ... [15]

radar dataset or in the wave characteristics in the locations were measurements were carried out only with SeaVision are welcome to request access from Alexander Gavrikov (gavr@sail.msk.ru).

Appendix A: List of the locations (stations) of the wind waves measurements during three research cruises

Table A1: Stations list: geographical locations and time of all stations where the wind waves measurements were performed simultaneously with SeaVision and Spotter buoy. In the last column letters stand for the name of the research vessel (ASV – Akademic Sergey Vavilov, AI – Akademic Ioffe) and numbers stand for the sequence number of reseach cruise since the beginnig of the reseach vessel operation.

#	Station #	Start UTC time	End UTC time	Latitude° N	Longitude° E	Cruise #
1	**2868**	27.08.2020 13:53	27.08.2020 14:13	65.67	-25.26	ASV50
2	**2881**	28.08.2020 10:45	28.08.2020 11:05	66.49	-28.89	ASV50
3	**2885**	28.08.2020 19:05	28.08.2020 19:25	66.84	-30.43	ASV50
4	**2763**	11.08.2020 11:25	11.08.2020 11:45	59.50	-10.00	ASV50
5	**2777**	13.08.2020 18:15	13.08.2020 18:35	59.50	-19.32	ASV50
6	**2782**	14.08.2020 18:42	14.08.2020 19:02	59.50	-22.66	ASV50
7	**2787**	15.08.2020 18:10	15.08.2020 18:30	59.50	-25.99	ASV50
8	**2797**	17.08.2020 10:12	17.08.2020 10:32	59.50	-32.67	ASV50
9	**2803**	18.08.2020 12:17	18.08.2020 12:37	59.50	-36.67	ASV50

Natalia 27.6.2022 21:44

Удалено: Dataset that contains significant wave height, wave periodwave energy frequency spectrum from both SeaVision and Spotter buoy at the locations of every station (Table A1, Gavrikov et al., 2022) is available through the PANGAEA repository (https://doi.org/10.1594/PANGAEA.939620). Users interested in the analysis of the raw radar dataset or in the wave characteristics in the locations were measurements were carried out only with SeaVision are welcome to request access from Alexander Gavrikov (gavr@sail.msk.ru).

10	**2809**	19.08.2020 13:26	19.08.2020 13:46	59.50	-40.34	ASV50
11	**2821**	20.08.2020 13:44	20.08.2020 14:04	59.90	-42.32	ASV50
12	**2833**	22.08.2020 15:26	22.08.2020 15:46	55.81	-34.47	ASV50
13	**2841**	23.08.2020 12:31	23.08.2020 12:51	56.78	-33.53	ASV50
14	**2849**	24.08.2020 14:06	24.08.2020 14:26	58.53	-31.43	ASV50
15	**2856**	25.08.2020 12:42	25.08.2020 13:02	60.30	-29.04	ASV50
16	**2863**	26.08.2020 11:45	26.08.2020 12:05	62.40	-25.73	ASV50
17	**2901**	30.08.2020 13:05	30.08.2020 13:25	65.94	-26.49	ASV50
18	**2903**	01.09.2020 13:05	01.09.2020 13:25	64.82	-12.49	ASV50
19	**2913**	02.09.2020 10:17	02.09.2020 10:37	63.35	-10.38	ASV50
20	**2928**	03.09.2020 19:24	03.09.2020 19:44	61.31	-8.25	ASV50
21	**2937**	04.09.2020 21:16	04.09.2020 21:36	59.50	-9.31	ASV50
22	**3831**	29.06.2021 19:49	29.06.2021 20:09	59.50	-4.60	AI57
23	**3841**	01.07.2021 09:26	01.07.2021 09:46	59.49	-11.33	AI57
24	**3847**	02.07.2021 10:33	02.07.2021 10:53	59.50	-15.33	AI57

25	**3853**	03.07.2021 12:35	03.07.2021 12:55	59.50	-19.33	AI57
26	**3858**	04.07.2021 11:38	04.07.2021 11:58	59.50	-22.67	AI57
27	**3863**	05.07.2021 10:05	05.07.2021 10:25	59.50	-26.00	AI57
28	**3870**	06.07.2021 16:29	06.07.2021 16:49	59.50	-30.67	AI57
29	**3875**	07.07.2021 15:57	07.07.2021 16:17	59.52	-33.98	AI57
30	**3880**	08.07.2021 17:32	08.07.2021 17:52	59.50	-37.33	AI57
31	**3884**	09.07.2021 13:51	09.07.2021 14:11	59.50	-40.00	AI57
32	**3899**	11.07.2021 12:45	11.07.2021 13:05	59.90	-42.48	AI57
33	**3911**	12.08.2021 13:27	12.08.2021 13:47	70.37	58.04	AI58
34	**3929**	14.08.2021 21:43	14.08.2021 22:03	75.15	75.09	AI58
35	**3930**	15.08.2021 06:40	15.08.2021 07:00	73.98	72.66	AI58
36	**3939**	16.08.2021 12:40	16.08.2021 13:00	73.75	73.66	AI58
37	**3946**	17.08.2021 04:53	17.08.2021 05:13	73.31	79.35	AI58
38	**3956**	18.08.2021 12:52	18.08.2021 13:12	75.14	79.54	AI58
39	**3972**	21.08.2021 12:27	21.08.2021 12:47	82.14	78.88	AI58

40	**3982**	22.08.2021 15:48	22.08.2021 16:08	81.93	73.70	AI58
41	**3990**	23.08.2021 14:43	23.08.2021 15:03	81.44	67.25	AI58
42	**3997**	24.08.2021 08:02	24.08.2021 08:22	81.04	72.66	AI58
43	**4013**	25.08.2021 19:28	25.08.2021 19:48	79.93	72.11	AI58
44	**4020**	26.08.2021 13:20	26.08.2021 13:40	79.51	65.06	AI58
45	**4025**	27.08.2021 03:05	27.08.2021 03:25	78.28	65.33	AI58
46	**4029**	27.08.2021 12:39	27.08.2021 12:59	77.67	65.45	AI58
47	**4031**	27.08.2021 18:30	27.08.2021 18:50	77.86	64.85	AI58
48	**4040**	28.08.2021 11:11	28.08.2021 11:31	78.84	61.62	AI58

Appendix B: Methodology for the computation of wave parameters from sea clutter images

We stated above (section 2.2.2) that to relate the signal to the wind waves, we assume that components of the spectrum outside of the dispersion relation are related to the background speckle-noise and components of the spectrum that satisfy the dispersion relation (1) related to the signal, associated with the wind waves. Eq. (1) presents the dispersion relation for the first harmonic and can be also easily extended to the second harmonic as follows:

$$\omega_{n,2}(k) = \sqrt{2gk} + 2k \cdot U \cdot cos\ \theta_n \qquad (B.1)$$

The curve associated with the second harmonic is clearly seen in Figure 3. The rest of the signal lying in the spectral domain outside the bands associated with dispersion curves and attributed to speckle-noise (Kanevsky, 2009) is needed to be properly quantified. This depends on the algorithm used for the quantification of bands associated with dispersion relation curves. Speckle-noise is used for normalization of the radar spectrum and removing the impulse power impact on the radar signal modulations by the sea waves (Kanevsky, 2009). The 2D normalized spectrum $S_{n,2d,norm}(k,f)$ of the signal at each wavenumber k can be calculated as:

$$S_{n,2d,norm}(k,f) = \frac{S_{n,2d,image}(k,f)}{\int S_{n,2d,image,\omega\,speckle}(k,f)df} - 1 \qquad \text{(B.2)}$$

where the speckle frequency is:

$$\omega_{speckle} = (f \notin \omega_{n,1}/2\pi \text{ } and \text{ } f \notin \omega_{n,2}/2\pi) \qquad \text{(B.3)}$$

Then the full image spectrum $S_{n,1,\omega}(f)$ needs to be filtered to obtain the power corresponding to the band capturing the first $\omega_{n,1}$ harmonic for the direction n:

$$S_{n,1,\omega}(f) = \int_{k_{n,1}-\Delta k}^{k_{n,1}+\Delta k} S_{n,2d,norm}(k,f)dk \qquad \text{(B.4)}$$

Here $k_{n,1}$ is the dispersion relation (1) solution for the first harmonic $\omega_{n,1}(k_{n,1}) = 2\pi f$ and Δk is related to the size of the processing area (720 m) as $\Delta k = 0.02 \approx 2 \cdot 2\pi/720$ (rad/m). Similarly for the second harmonic $\omega_{n,2}$ we obtain:

$$S_{n,2,\omega}(f) = \int_{k_{n,2}-\Delta k}^{k_{n,2}+\Delta k} S_{n,2d,norm}(k,f)dk \qquad \text{(B.5)}$$

where $k_{n,2}$ is the dispersion relation (B1) solution for the second harmonic $\omega_{n,2}(k_{n,2}) = 2\pi f$.

The total power $S_{n,\omega}(f)$ falling in the bands along dispersion relation curves yields:

$$S_{n,\omega}(f) = S_{n,1,\omega}(f) + S_{n,2,\omega}(f) \qquad \text{(B.6)}$$

Given that this procedure is applied to all 16 sectors of the image (see section 2.2.2), the omnidirectional image frequency spectrum $S_{image}(f)$ can be derived as follows:

$$S_{image}(f) = \frac{1}{16}\sum_{n=1}^{16} S_{n,\omega}(f) \qquad \text{(B.7)}$$

Further integration over the frequency domain returns the zeroth moment $m_{0,image}$ of the $S_{image}(f)$ spectrum:

$$m_{0,image} = \int_0^\infty S_{image}(f)df, \qquad \text{(B.8)}$$

which provides us with the estimate of *SNR* being:

$$SNR \equiv m_{0,image} + 1.$$

Formally, considering the $S_{image,\omega}(f)$ spectrum as a modulation analog of the real sea wave spectrum, $S_w(f)$, the zeroth moment $m_{0,image}$ can be further converted to the magnitude of signal modulations H_{image} on the radar image which stands as a provisional measure of H_s:

$$H_{image} = 4\sqrt{m_{0,image}} \qquad \text{(B.9)}$$

Further the transform of the omnidirectional SeaVision image frequency spectrum $S_{image}(f)$ to the sea wave frequency (wave energy) spectrum $S_{w,SeaVision}(f)$ visible by SeaVision is performed by applying the standard technique described in section 2.2.2 and resulting in Eq. (2) returning significant wave height $\mathrm{H_{s,SeaVision}}$ estimate based on the radar calibration coefficients A and B along with estimate for the wind wave period (4) derived from the zeroth and the first moments of the spectrum.

Appendix C: Definition of all the parameters in the manuscript and dataset.

Parameters	Short name	Definition	Range	Name in netcdf
Meteorological variables				
Wind Speed $(m \cdot s^{-1})$	U_{10}	-	-	meteo_wspd
Wind Direction (°)	θ_{10}	-	0 – 360° (from)	meteo_wdir
Atmospheric Pressure (hPa)	p	-	-	meteo_pres
Atmospheric Temperature (°C)	T	-	-	meteo_temp
Humidity (%)	H	-	0 – 100 %	meteo_humd
Spotter wave buoy variables				
1-D wave energy spectrum $(m^2 \cdot Hz^{-1})$	$S_{w,Spotter}$	$\int_{f4}^{f127} S(f)df$	0.0391 – 1.25 Hz	buoy_Szz, buoy_freq
Significant Wave Height (m)	$H_{s,Spotter}$	$4\sqrt{m_0}$	0.2 – 4.2 m	buoy_hs
Energy Wave Period (s)	$T_{m01,Spotter}$	$\frac{m_0}{m_1}$	1.85 – 8.85 s	buoy_ts
Mean Wave Direction (°)	$D_{s,Spotter}$	$270^0 - \frac{180^0}{\pi} arctan\,2(b_1, a_1)$	0 – 360° (from)	buoy_ds
SeaVision variables				
1-D wave energy spectrum $(m^2 \cdot Hz^{-1})$	$S_{w,SeaVision}$	$\int_0^{360} S(k,f)dk$	0.0423 – 0.4069 Hz	radar_Szz radar_freq
Significant Wave Height (m)	$H_{s,SeaVision}$	$4\sqrt{m_0}$	0.3 – 3 m	radar_hs
Energy Wave Period (s)	$\mathrm{T_{m01,SeaVision}}$	$\frac{m_0}{m_1}$	3.7 – 8.5 s	radar_ts

Mean Wave Direction (°)	$D_{s,SeaVision}$	$270^0 - \frac{180^0}{\pi} arctan\,2(b_1, a_1)$	0 – 360° (from)	radar_ds

Author contributions

NT, AG, DI, VS, AS, LS, VS and PS participated in research cruises and data collection. The leading role in field work program development and implementation belongs to AG and VS. DI made preprocessing, postprocessing and analysis of the radar (SeaVision) dataset, VS developed the configuration and ran the WW3 model for the period of cruises, AG analysed all Spotter buoy data. EE, AG and VS did validation with satellite missions. VF, BT and SB provided hardware development and mounting of the SeaVision to the research vessels. VT, OR and AS provided operational support for the research cruises. NT has a leading role in the project set up and manuscript writing. The initial idea of the research belongs to SG. The scoping of the manuscript was developed by NT, SG and KPK. All authors contributed to the discussion, interpretation of the results and writing.

Natalia 27.6.2022 21:45

Удалено: NT, AG, DI, VS, AS, LS, VS and PS participated in research cruises and data collection. The leading role in field work program development and implementation belongs to AG and VS. DI made preprocessing, postprocessing and analysis of the radar (SeaVision) dataset, VS developed the configuration and ran the WW3 model for the period of cruises, AG analysed all Spotter buoy data. EE, AG and VS did validation with satellite missions. VF, BT and SB provided hardware development and mounting of the SeaVision to the research vessels. VT, OR and AS provided operational support for the cruises in which SeaVision was used. NT has a leading role in the project set up and manuscript writing. The initial idea of the research belongs to SG. The scoping of the manuscript was developed by NT, SG and KPK. All authors contributed to the discussion, interpretation of the results and writing.

Competing interests

The authors declare no conflict of interests.

Acknowledgements

We thank anonymous Reviewer 1 and Alamgir Hossan (Reviewer 2) for careful examination of the manuscript and useful comments and suggestions that allowed to improve the manuscript significantly. We also thank Ian Young and Vladimir Karaev for their comments during the open discussion stage. We acknowledge Igor Skvortsov and the Atlantic branch of the Shirshov Institute of Oceanology in Kaliningrad for the local support and the crews of research vessels "*Akademik Sergey Vavilov*" and "*Akademik Ioffe*" for their help in setting up buoy measurements in the open ocean. We are also thankful to Vika Grigorieva and Igor Goncharenko of Shirshov Institute of Oceanology for their help with setting up the hardware for radar signal digitization and useful advice. We thank Takaya Uchida at Université Grenoble Alpes for final proofreading of the manuscript.

Natalia 27.6.2022 21:45

Удалено: We thank Anonymous Reviewer 1 and Alamgir Hossan as Reviewer 2 for careful examination of the manuscript and useful comments and suggestions that allowed to improve the manuscript significantly. We also thank Ian Young and Vladimir Karaev for their comments during the open discussion. We acknowledge Skvortsov Igor and the Atlantic branch of the Shirshov Institute of Oceanology in Kaliningrad for their local support and crew of research vessels *Akademik Sergey Vavilov* and *Akademic Ioffe* for their help in setting up buoy measurements in the open ocean. We are also thankful to Viktoriya Grigorieva and Igor Goncharenko from Shirshov Institute of Oceanology for their help with setting up hardware for radar signal digitization and useful advices. We also thank Takaya Uchida at Université Grenoble Alpes for final proofreading of the manuscript.

Financial support

This study was funded by the Russian Foundation for Basic Research, project № 20-35-70025. VS and AG were also supported with grant № 17-77-20112-P from the Russian Science Foundation (WW3 setting for the period of the research cruises). SG was supported by the Ministry of Science and Higher Education of the Russian Federation (agreement 075-15-2021-577, interpretation and analysis of observational biases).

References

An J., Huang W., and Gill E. W.: “A self-adaptive wavelet-based algorithm for wave measurement using nautical radar,” IEEE Transactions on Geoscience and Remote Sensing, vol. 53, no. 1, pp. 567–577, 2015.

Andreas, E. L.: Fallacies of the enthalpy transfer coefficient over the ocean in high winds. Journal of the Atmospheric Sciences, 68, 1435-1445, https://doi.org/10.1175/2011JAS3714.1, 2011.

Babanin, A. V.: On a wave-induced turbulence and a wave-mixed upper ocean layer. Geophys. Res. Lett., 33, L20605. doi:10.1029/2006GL027308, 2006.

Babanin, A.V.: Breaking and Dissipation of Ocean Surface Waves. Cambridge University Press, 2011.

Blomquist, B. W., Brumer, S. E., Fairall, C. W., Huebert, B. J., Zappa, C. J., Brooks, I. M., … Pascal, R. W.: Wind speed and sea state dependencies of air-sea gas transfer: Results from the high wind speed gas exchange study (HiWinGS). Journal of Geophysical Research: Oceans, 122, 8034– 8062, https://doi.org/10.1002/2017JC013181, 2017

Buckingham, C. E., Lucas, N. S., Belcher, S. E., Rippeth, T. P., Grant, A. L. M., Lesommer, J., et al.: The contribution of surface and submesoscale processes to turbulence in the open ocean surface boundary layer. Journal of Advances in Modeling Earth Systems, 11, 4066– 4094. https://doi.org/10.1029/2019MS001801, 2019

Buckley, J. R. and Aler, J.: Enhancements in the determination of ocean surface wave height from grazing incidence microwave backscatter, in International Geoscience and Remote Sensing Symposium (IGARSS), vol.5.,https://doi.org/10.1109/IGARSS.1998.702254, 1998.

Buckley, J. R. and Aler, J.: Estimation of ocean wave height from grazing incidence microwave backscatter, in International Geoscience and Remote Sensing Symposium (IGARSS),vol. 2., https://doi.org/10.1109/IGARSS.1997.615328, 1997.

Campana, J., Terrill, E. J. and Paolo, T. de: A new inversion method to obtain upper-ocean current-depth profiles using X-band observations of deep-water waves, Journal of Atmospheric and Oceanic Technology, 34(5), https://doi.org/10.1175/JTECH-D-16-0120.1, 2017.

Casas-Prat, M., Wang, X.L., and Swart, N.: CMIP5-based global wave climate projections including the entire Arctic Ocean, Ocean Modelling, 123, 66-85, 2018.

Cavaleri, L., Fox-Kemper B., and Hemer M.: Wind waves in the coupled climate system. Bull. Amer. Meteor. Soc., 93, 1651–1661, 2012.

Cavaleri, L., Barbariol, F. and Benetazzo, A.: Wind-wave modeling: Where we are, where to go, Journal of Marine Science and Engineering, 8(4), https://doi.org/10.3390/JMSE8040260, 2020.

Chen, Z., He, Y., Zhang, B., & Qiu, Z. (2015). Determination of nearshore sea surface wind vector from marine X-band radar images. *Ocean Engineering*, *96*, 79–85,https://doi.org/10.1016/J.OCEANENG.2014.12.019, 2015.

Chen, Z., Zhang, B., Kudryavtsev, V., He, Y., & Chu, X. (2019). Estimation of sea surface current from X-band marine radar images by cross-spectrum analysis. *Remote Sensing*, *11*(9), https://doi.org/10.3390/rs11091031, 2019.

Crombie, D. D.: Doppler spectrum of sea echo at 13.56 Mc./s. [3], Nature, 175(4459), https://doi.org/10.1038/175681a0, 1955.

Cronin M.F., Gentemann C.L., Edson J., Ueki I., Bourassa M., Brown S., Clayson C.A., Fairall C.W., Farrar J.T., Gille S.T., Gulev S., Josey S.A., Kato S., Katsumata M., Kent E., Krug M., Minnett P.J., Parfitt R., Pinker R.T., Stackhouse P.W. Jr, Swart S., Tomita H., Vandemark D., Weller R.A., Yoneyama K., Yu L. and Zhang D.: Air-Sea Fluxes With a Focus on Heat and Momentum. Front. Mar. Sci. 6:430. doi: 10.3389/fmars.2019.00430, 2019

Dankert, H. and Horstmann, J.: A marine radar wind sensor, Journal of Atmospheric and Oceanic Technology, 24(9), https://doi.org/10.1175/JTECH2083.1, 2007.

Dankert, H., Horstmann, J. and Rosenthal, W.: Ocean wind fields retrieved from radar-image sequences, Journal of Geophysical Research: Oceans, 108(11), https://doi.org/10.1029/2003jc002056, 2003.

Derkani, M. H., Alberello, A., Nelli, F., Bennetts, L. G., Hessner, K. G., Machutchon, K., Reichert, K., Aouf, L., Khan, S. and Toffoli, A.: Wind, waves, and surface currents in the Southern Ocean: Observations from the Antarctic Circumnavigation Expedition, Earth System Science Data, 13(3), https://doi.org/10.5194/essd-13-1189-2021, 2021.

Drouet, C., Cellier, N., Raymond, J. and Martigny, D.: Sea state estimation based on ship motions measurements and data fusion, in Proceedings of the International Conference on Offshore Mechanics and Arctic Engineering - OMAE, vol. 5., Nantes, France, 9–14 June 2013, OMAE2013-10657, https://doi.org/10.1115/OMAE2013-10657, 2013.

Fan, Y., and Griffies, S. M.: Impacts of Parameterized Langmuir Turbulence and Nonbreaking Wave Mixing in Global Climate Simulations. Journal of Climate 27, 12, 4752-4775, https://doi.org/10.1175/JCLI-D-13-00583.1, 2014.

Gangeskar, R.: An algorithm for estimation of wave height from shadowing in X-band radar sea surface images, IEEE Transactions on Geoscience and Remote Sensing, 52(6), http://dx.doi.org/10.1109/TGRS.2013.2272701, 2014.

Gangeskar, R.: Wave height derived by texture analysis of X-band radar sea surface images, in International Geoscience and Remote Sensing Symposium (IGARSS), vol. 7., https://doi.org/10.1109/IGARSS.2000.860301, 2000.

Gavrikov, Alexander; Ivonin, Dmitry; Sharmar, Vitaly; Tilinina, Natalia; Gulev, Sergey; Suslov, Alexander; Fadeev, Vladimir; Trofimov, Boris; Bargman, Sergey; Salavatova, Leysan; Koshkina, Vasilisa; Shishkova, Polina; Sokov, Alexey (2021): Wind waves in the North Atlantic and Arctic from ship navigational radar (SeaVision system) and wave buoy Spotter during three research cruises in 2020 and 2021. PANGAEA, https://doi.pangaea.de/10.1594/PANGAEA.939620 (dataset in review)

Greenwood C., Vogler A., Morrison J., Murray A.: The approximation of a sea surface using a shore mounted X-band radar with low grazing angle. Remote Sensing of Environment, 204, 439-447, https://doi.org/10.1016/j.rse.2017.10.012, 2018.

Gulev, S.K. and Hasse L.: North Atlantic wind waves and wind stress from voluntary observing data. J. Phys.Oceanogr., 28, 1107-1130, 1998.

Gulev, S.K., Grigorieva V., Sterl A., and Woolf D.: Assessment of the reliability of wave observations from voluntary observing ships: insights from the validation of a global wind wave climatology based on voluntary observing ship data. J. Geophys. Res. – Oceans, 108(C7), 3236. doi:10,1029/2002JC001437, 2003.

Hasselmann, K.: Theory of synthetic aperture radar ocean imaging: a MARSEN view., Journal of Geophysical Research, 90(C3), https://doi.org/10.1029/JC090iC03p04659, 1985.

Hasselmann, S., Hasselmann, K., Allender, J. H. and Barnett, T. P.: Computations and parameterizations of the nonlinear energy transfer in a gravity-wave spectrum. Part II: parameterizations of the nonlinear energy transfer for application in wave models., J. PHYS. OCEANOGR., 15(11, Nov. 1985), https://doi.org/10.1175/1520-0485(1985)015<1369:CAPOTN>2.0.CO;2, 1985.

Hatten, H., Seemann, J., Horstmann, J. and Ziemer, F.: Azimuthal dependence of the radar cross section and the spectral background noise of a nautical radar at grazing incidence, in International Geoscience and Remote Sensing Symposium (IGARSS), vol. 5.,https://doi.org/10.1109/IGARSS.1998.702255,1998.

Hersbach, H., Bell, B., Berrisford, P., Hirahara, S., Horányi, A., Muñoz Sabater, J., ... & Thépaut, J. N.: The ERA5 global reanalysis, Quarterly Journal of the Royal Meteorological Society, 146(730), 1999-2049, https://doi.org/10.1002/qj.3803, 2020.

Hessner K., Reichert K., Dittmer J. Nieto Borge and Günther H.:Ocean Wave Measurement and Analysis, https://doi.org/10.1061/40604(273)23, 2001.

Hessner, K. and Hanson, J. L.: Extraction of coastal wavefield properties from X-band radar, in International Geoscience and Remote Sensing Symposium (IGARSS), https://doi.org/10.1109/IGARSS.2010.5650134, 2010.

Hilmer, T. and Thornhill, E.: Observations of predictive skill for real-time Deterministic Sea Waves from the WaMoS II, in OCEANS 2015 - MTS/IEEE Washington., 2016.

Huang W., Gill E. W., and An J.: Iterative least-squares-based wave measurement using X-band nautical radar, IET Radar, Sonar & Navigation, vol. 8, no. 8, pp. 853–863, 2014.

Hwang, P. A., Sletten, M. A. and Toporkov, J. V.: A note on Doppler processing of coherent radar backscatter from the water surface: With application to ocean surface wave measurements, Journal of Geophysical Research: Oceans, 115(3), https://doi.org/10.1029/2009JC005870, 2010.

Ivonin, D.V., Telegin, V.A., Chernyshov, P.V. et al. Possibilities of X-band nautical radars for monitoring of wind waves near the coast. Oceanology 56, 591–600, https://doi.org/10.1134/S0001437016030103, 2016.

Johnson, J. T., Burkholder, R. J., Toporkov, J. V., Lyzenga, D. R. and Plant, W. J.: A numerical study of the retrieval of sea surface height profiles from low grazing angle radar data, in IEEE Transactions on Geoscience and Remote Sensing, vol. 47., https://doi.org/10.1109/IGARSS.2010.5650134, 2009.

Kanevsky M.B.: Radar Imaging of the Ocean Waves, Elsevier, ISBN 9780444532091, https://doi.org/10.1016/B978-0-444-53209-1.00010-1. pp. 179-180, 2009

Karaev, V.Y., Kanevsky, M.B., Meshkov, E.M. et al.: Measurement of the variance of water surface slopes by a radar: Verification of algorithms. Radiophys Quantum El 51, 360 https://doi.org/10.1007/s11141-008-9042-6, 2008.

McWilliams, J., & Fox-Kemper, B.: Oceanic wave-balanced surface fronts and filaments. Journal of Fluid Mechanics, 730, 464-490. doi:10.1017/jfm.2013.348, 2013.

Morim, J., Trenham, C., Hemer, M. et al.:A global ensemble of ocean wave climate projections from CMIP5-driven models. Sci Data 7, 105. https://doi.org/10.1038/s41597-020-0446-2, 2020.

Morim, J., Erikson, L.H., Hemer, M. et al. A global ensemble of ocean wave climate statistics from contemporary wave reanalysis and hindcasts. Sci Data 9, 358 https://doi.org/10.1038/s41597-022-01459-3, 2022.

Nagai, T., Satomi, S., Terada, Y., Kato, T., Nukada, K. and Kudaka, M.: GPS buoy and seabed installed wave gauge application to offshore tsunami observation, in Proceedings of the International Offshore and Polar Engineering Conference, vol. 2005., Seoul, Korea, 19–24 June 2005,ISOPE-I-05-282, available at: https://onepetro.org/ISOPEIOPEC/proceedings-abstract/ISOPE05/All-ISOPE05/ISOPE-I-05-282/9448, 2005.

Nieto Borge J.C., Reichert K., Dittmer, J.:Use of nautical radar as a wave monitoring instrument, Coastal Engineering, Vol.37, pp. 331-342, 1999.

Nieto-Borge, J. C. and Guedes Soares, C.: Analysis of directional wave fields using X-band navigation radar, Coastal Engineering, 40(4), https://doi.org/10.1016/S0378-3839(00)00019-3, 2000.

Nieto-Borge, J. C., Hessner, K., Jarabo-Amores, P. and De La Mata-Moya, D.: Signal-to-noise ratio analysis to estimate ocean wave heights from X-band marine radar image time series, IET Radar, Sonar and Navigation, 2(1), https://doi.org/10.1049/iet-rsn:20070027, 2008.

Nieto-Borge, J. C., Jarabo-Amores, P., De La Mata-Moya, D. and López-Ferreras, F.: Estimation of ocean wave heights from temporal sequences of X-band marine radar images, in European Signal Processing Conference., Lüneburg, Germany 4–9 June 2006, 35 – 41, https://doi.org/10.1115/OMAE2006-92015, 2006.

Park, G. I., Choi, J. W., Kang, Y. T., Ha, M. K., Jang, H. S., Park, J. S., Kwon, S. H.: The application of marine X-band radar to measure wave condition during sea trial. Journal of Ship and Ocean Technology, 10(4), 34-48, available at: https://www.koreascience.or.kr/article/JAKO200614539116884.page, 2006.

Plant, W. J., Keller, W. C., Reeves, A. B., Uliana, E. A. and Johnson, J. W.: Airborne microwave doppler measurements of ocean wave directional spectra, International Journal of Remote Sensing, 8(3), https://doi.org/10.1080/01431168708948644, 1987.

Plant, W. J.: A model for microwave Doppler sea return at high incidence angles: Bragg scattering from bound, Tilted waves, Journal of Geophysical Research: Oceans, 102(C9), https://doi.org/10.1029/97JC01225, 1997.

Raghukumar, K., Chang, G., Spada, F., Jones, C., Janssen, T. and Gans, A.: Performance characteristics of “spotter,”' a newly developed real-time wave measurement buoy, Journal of Atmospheric and Oceanic Technology, 36(6), https://doi.org/10.1175/JTECH-D-18-0151.1, 2019.

Reichert, K., Hessner, K., Dannenberg, J. and Traenkmann, I.: X-Band radar as a tool to determine spectral and single wave properties, in Proceedings of the International Conference on Offshore Mechanics and Arctic Engineering - OMAE, vol. 2006., Hamburg, Germany, 4–9 June 2006, 683-688, https://doi.org/10.1115/OMAE2006-92015, 2006.

Ribal, A. and Young, I. R.: Publisher Correction: 33 years of globally calibrated wave height and wind speed data based on altimeter observations (Scientific Data, (2019), 6, 1, (77), 10.1038/s41597-019-0083-9), Scientific Data, 6(1), https://doi.org/10.1038/s41597-019-0108-4, 2019.

Ribas-Ribas M., Helleis F., Rahlff. J and Wurl O.: Air-Sea CO2-Exchange in a Large Annular Wind-Wave Tank and the Effects of Surfactants. Front. Mar. Sci. 5:457. doi: 10.3389/fmars.2018.00457, 2018.

Rogers, W. E., Babanin, A. V. and Wang, D. W.: Observation-consistent input and whitecapping dissipation in a model for wind-generated surface waves: Description and simple calculations, Journal of Atmospheric and Oceanic Technology, 29(9), https://doi.org/10.1175/JTECH-D-11-00092.1, 2012.

Seemann, J., Ziemer, F. and Senet, C. M.: Method for computing calibrated ocean wave spectra from measurements with a nautical X-band radar, in Oceans Conference Record (IEEE), vol. 2., Halifax, NS, Canada, 6-9 October 1997, https://doi.org/10.1109/OCEANS.1997.624154, 1997.

Semedo, A., Dobrynin, M., Lemos, G., Behrens, A., Staneva, J., de Vries, H., … Murawski, J.: CMIP5-Derived Single-Forcing, Single-Model, and Single-Scenario Wind-Wave Climate Ensemble: Configuration and Performance Evaluation. Journal of Marine Science and Engineering, 6(3), 90. doi:10.3390/jmse6030090, 2018.

Senet, C. M., Seemann, J. and Ziemer, F.: The near-surface current velocity determined from image sequences of the sea surface, IEEE Transactions on Geoscience and Remote Sensing, 39(3), https://doi.org/10.1109/36.911108, 2001.

Sharmar, V., Markina M., Gulev S.K.: Global Ocean Wind-Wave Model Hindcasts Forced by Different Reanalyzes: A Comparative Assessment Journal of Geophysical Research: Oceans, 126, e2020JC016710. https://doi.org/10.1029/2020JC016710, 2021.

Smit P.B., Houghton I.A., Jordanova K., Portwood T., Shapiro E., Clark D., Sosa M., Janssen T.T.: Assimilation of significant wave height from distributed ocean wave sensors Ocean Model, 15, p. 101738, https://doi.org/10.1016/j.ocemod.2020.101738, 2021.

Story, W. R., Fu, T. C. and Hackett, E. E.: Radar measurement of ocean waves, in Proceedings of the International Conference on Offshore Mechanics and Arctic Engineering - OMAE, vol. 6., https://doi.org/10.1115/OMAE2011-49895, 2011.

Studholme, J., Fedorov A. V., Gulev S. K., Emanuel K. and Hodges K.: Poleward expansion of tropical cyclone latitudes in warming climates Nature Geoscience, https://doi.org/10.1038/s41561-021-00859-1, 2021.

Swail,V., Jensen, R.E., Lee, B., Turton, J., Thomas, J., Gulev, S., Yelland, M., Etala, P., Meldrum, D., Birkemeier, W., Burnett B. and Warren G.: Wave Measurements, Needs and Developments for the Next Decade., available at: http://waveworkshop.org/11thWaves/Papers/Swail_etal_Wave%20Measurements.pdf, 2010.

WAMDI Group, T. W. (1988). The WAM Model—A Third Generation Ocean Wave Prediction Model. Journal of Physical Oceanography 18, 12, 1775-1810, https://doi.org/10.1175/1520-0485, 1988.

The WAVEWATCH III Development Group (WW3DG), (2019): User manual and system documentation of WAVEWATCH III R version 6.07. Tech. Note 333, NOAA/NWS/NCEP/MMAB, College Park, MD, USA, 465 pp. + Appendices., available at: https://github.com/NOAA-EMC/WW3/wiki/Manual, 2019.

Verezemskaya, P., Barnier, B., Gulev, S. K., Gladyshev, S., Molines, J. M., Gladyshev, V., Lellouche, J. M. and Gavrikov, A.: Assessing Eddying (1/12°) Ocean Reanalysis GLORYS12 Using the 14-yr Instrumental Record From 59.5°N Section in the Atlantic, Journal of Geophysical Research: Oceans, 126(6), https://doi.org/10.1029/2020JC016317, 2021.

Vicen-Bueno, R., Horstmann, J., Terril, E., de Paolo, T. and Dannenberg, J.: Real-time ocean wind vector retrieval from marine radar image sequences acquired at grazing angle, Journal of Atmospheric and Oceanic Technology, 30(1), https://doi.org/10.1175/JTECH-D-12-00027.1, 2013.

Vicen-Bueno, R., Lido-Muela, C. and Nieto-Borge, J. C.: Estimate of significant wave height from noncoherent marine radar images by multilayer perceptrons, Eurasip Journal on Advances in Signal Processing, 2012(1), https://doi.org/10.1186/1687-6180-2012-84, 2012.

Xu, J., and Wang, Y.: Potential Intensification Rate of Tropical Cyclones in a Simplified Energetically Based Dynamical System Model: An Observational Analysis. Journal of the Atmospheric Sciences 79, 4, 1045-1055, https://doi.org/10.1175/JAS-D-21-0217.1, 2022.

Young, I. R., Rosenthal, W. and Ziemer, F.: A three-dimensional analysis of marine radar images for the determination of ocean wave directionality and surface currents., Journal of Geophysical Research, 90(C1), https://doi.org/10.1029/JC090iC01p01049, 1985.

Zieger S., Babanin A. V., Rogers W. E., and Young I. R. (2015), Observation-based source terms in the third-generation wave model WAVEWATCH. Ocean Modelling., 96, 2-25.

Natalia 27.6.2022 21:45

Удалено: Borge, J. C. N., Reichert, K. and Dittmer, J.: Use of nautical radar as a wave monitoring instrument, Coastal Engineering, 37(3–4), https://doi.org/10.1016/S0378-3839(99)00032-0,1999. ... [16]